

DYNAMICS OF THE N₂O LASER AS MEASURED WITH A TDL

DYNAMICS OF THE N₂O LASER AS MEASURED
WITH A TUNABLE DIODE LASER

By

KAREN ELIZABETH FOX, B.Sc.

A Thesis

Submitted to the School of Graduate Studies
in Partial Fulfilment of the Requirements
for the Degree
Master of Science

McMaster University

October 1984

MASTER OF SCIENCE (1984)
(Physics)

McMASTER UNIVERSITY
Hamilton, Ontario

TITLE: Dynamics of the N_2O Laser as Measured with a Tunable
Diode Laser

AUTHOR: Karen Elizabeth Fox, B.Sc. (University of Waterloo)

SUPERVISOR: Professor J. Reid, Professor P. Jessop

NUMBER OF PAGES: x, 80

ABSTRACT

The work presented in this thesis was undertaken to explain the differences in output powers and small-signal gain coefficients observed in cw N_2O and CO_2 lasers. To isolate the factors limiting small-signal gain, the dynamics of conventional cw N_2O laser discharges were investigated using a tunable diode laser (TDL) operating in the 2120-2350 cm^{-1} frequency region. Absorption measurements were made with the TDL on more than 10 different vibrational bands, allowing vibrational population distributions in the three normal modes of vibration of N_2O to be determined. The vibrational populations follow a Boltzmann distribution, and the ν_1 and ν_2 mode temperatures are found to be strongly coupled, and to maintain equilibrium with the background gas temperature under all discharge conditions. It is observed that the ν_3 mode temperature saturates at high discharge currents. This saturation, which is attributed to electron de-excitation, is determined to be the primary factor limiting small-signal 10- μm gain in the N_2O laser and is much more important than N_2O dissociation. The maximum small-signal gain coefficients achievable in cw N_2O lasers are calculated, and the results of the work indicates the measures that must be taken to optimize small-signal gain in the N_2O laser.

ACKNOWLEDGEMENTS

I would like to express my sincere appreciation to my supervisor Dr. John Reid for his teaching and guidance during this work. I am also indebted to my co-supervisor Dr. Paul Jessop for his comments and suggestions during many conversations.

Financial support from NSERC and the McMaster University Department of Physics is gratefully acknowledged.

Lastly, I extend deep thanks to my friends, my parents and my grandparents for their patience when my letters and visits came too infrequently during the course of this work.

TABLE OF CONTENTS

	<u>PAGE</u>
ABSTRACT	iii
ACKNOWLEDGEMENTS	iv
CHAPTER	
1. INTRODUCTION	1
2. THEORY	4
2.1 Introduction	4
2.2 Spectroscopy of N ₂ O	5
2.3 Excitation and Energy Transfer Mechanisms	14
2.3.1 Excitation of N ₂ O(00 ⁰ 1)	15
2.3.2 Relaxation Processes	16
2.4 The Mode-Temperature Model	20
2.5 Calculation of the Absorption Coefficient	23
2.6 Summary	29
3. EXPERIMENTAL APPARATUS AND MEASUREMENT TECHNIQUES	31
3.1 The Experimental System	31
3.2 Mode Temperature Determination and Initial Results	35
3.2.1 Rotational Temperatures	36
3.2.2 Vibrational Temperatures	38
3.3 Summary	43
4. DISSOCIATION OF N ₂ O	46
4.1 Experimental Procedure	46
4.2 Dissociation Results	49
4.3 Summary	52
5. MODE TEMPERATURES IN N ₂ O DISCHARGES	53
5.1 Results	53
5.2 Summary	58
6. 10- μ m GAIN CALCULATIONS	59
6.1 Results	59
6.2 Discussion	61
6.3 Summary	66

7. CONCLUSIONS	67
APPENDIX I	70
REFERENCES	75

LIST OF FIGURES

<u>FIGURE</u>	<u>PAGE</u>
2.1 The normal modes of vibration of the N ₂ O molecule. The vibrational frequencies and symmetry types (species) are also indicated.	6
2.2 Partial vibrational energy level diagram for N ₂ O showing the three fundamental modes with their associated mode temperatures. Also shown are some typical transitions in the 2200 cm ⁻¹ region that are probed with the tunable diode laser.	8
2.3 The rotational sub-structure superimposed upon the vibrational energy levels is shown for two different vibrational symmetry species, e.g., the 00 ⁰ 0 (Σ) and 01 ¹ 0 (Π) modes.	10
2.4 Typical rotational-vibrational spectrum showing the P and R branches of the fundamental band (00 ⁰ 1-00 ⁰ 0). Transitions between vibrational levels also involve a change in rotational quantum number J. The spectral transitions are labelled by the J value of the lower level, e.g., 00 ⁰ 0 J=4 → 00 ⁰ 1 J=5 produces the R(4) line.	13
3.1 Schematic diagram of the experimental apparatus.	32
3.2 Typical TDL scans recorded with the laser beam focussed into the discharge tube. The upper scan is taken with no discharge current, while the lower scan corresponds to a current of 15 mA in a 15%N ₂ O:15%N ₂ :70%He mixture at 13.7 Torr. The more important absorption lines are labelled beneath the traces. Bracketed numbers indicate isotopes other than the most abundant ¹⁴ N ¹⁴ N ¹⁶ O isotope, .e.g., ¹⁵ N ¹⁴ N ¹⁶ O is labelled (546). Each transition is identified by its lower vibrational level. ⁵⁷	34
3.3 Rotational distributions measured in the 00 ⁰ 0 band of ¹⁵ N ¹⁴ N ¹⁶ O at room temperature, and the 00 ⁰ 2 band of ¹⁴ N ₂ ¹⁶ O at a discharge current of 25 mA. The pressure was 13.7 Torr. The smooth curves show the theoretical calculations; the distributions are normalized to a maximum value of unity.	38
3.4 Vibrational population distributions in the ν ₃ mode of	40

FIGUREPAGE

- N_2O at discharge currents of 5 mA and 25 mA. Data points are experimental measurements made with the TDL, while the solid line is a linear fit, constrained to pass through the point (0,0). The slope of the line gives the mode temperature, T_3 .
- 3.5 Repeat of Fig. 3.4 for a 15% N_2O :15% N_2 :70%He mixture. Note the drop in T_3 which occurs as the N_2O content is increased from the value of 2% in Fig. 3.4. 41
- 3.6 Vibrational population distributions in the v_1 and v_2 modes of N_2O at discharge currents of 5 and 25 mA. Data points are experimental measurements for the levels indicated in the figure, while the solid lines represent Boltzmann distributions for the indicated value of $T_1=T_2$. 44
- 4.1 Schematic diagram showing the 0.8-cm-long cell situated at the outlet of the discharge. This short cell is used to measure absorption coefficients on the $^{14}N^{14}N^{16}O$ isotope fundamental lines in order to determine the magnitude of dissociation in the discharge. 47
- 4.2 Degree of N_2O dissociation measured at the outlet of the discharge tube as a function of the discharge current and flowrate. The measurements were made on the $00^0_0 P(44)$ lines of the $^{14}N^{14}N^{16}O$ isotope. 50
- 4.3 Degree of N_2O dissociation measured at the outlet of the discharge tube as a function of inlet gas mixture and current. Dwell time in the discharge was ~11 msec and the total pressure was 13.7 Torr. The associated absorption measurements were made on a variety of different transitions. 51
- 5.1 Experimental values of T_3 , $T_2(=T_1)$ and T as a function of discharge current. The gas flow rate is 773 ml/min NTP, resulting in a gas dwell time in the discharge region of ~11 msec. 54
- 5.2 Repeat of Fig. 5.1 for a 15% N_2O :15% N_2 :70%He mixture. The gas flow rate is 399 ml/min NTP, resulting in a gas dwell time in the discharge region of ~21 msec. 55
- 5.3 T_3 measurements as a function of gas mixture in both N_2O and CO_2 discharges. The CO_2 curve is taken from Ref. 63 and represents the average of many pulsed and cw measurements taken under conditions designed to maximize T_3 . The N_2O data points were measured in the present work; the cw measurements (circles) were made with a TDL for a mixture containing 15% N_2 at a total pressure of 13.7 Torr and a discharge current of 10 mA. The pulsed

FIGURE

PAGE

measurements (squares) were made in a transversely-excited discharge using the techniques described in Ref. 63. $T(=T_1=T_2)$ is also shown as a function of gas mixture for N_2O .

- 6.1 Calculated 10- μ m gain on the P(20) transition of the $00^0_1-00^0_0$ band for two different N_2O mixtures at 13.7 Torr. The solid lines join calculated points for which dissociation is included; the dashed lines show gain calculated by assuming that the measured temperatures correspond to the undissociated mixtures. Dissociation estimates are an average over the 10-cm discharge length, as outlined in Chapter 4. 60
- 6.2 Calculated 10- μ m gain as a function of effective % N_2O in the gas mixture at 13.7 Torr. The mixtures were prepared with 15% N_2 and the balance was helium. The associated TDL measurements were taken at a discharge current of 10 mA, and the calculations were carried out using the data of Figs. 4.3 and 5.3. 62

LIST OF TABLES

<u>TABLE</u>		<u>PAGE</u>
2.1	Molecular Constants Used For N ₂ O Transition Frequency Calculations	12
2.2	Vibrational Matrix Elements and F _J Values for N ₂ O	25
2.3	Expressions for S _J , the Rotational Contribution to the Spontaneous Transition Probability	26
2.4	Collision-Broadening Coefficients for N ₂ O	28
6.1	Comparison of 10- μ m Gain in cw N ₂ O and CO ₂ Systems	63

CHAPTER 1

INTRODUCTION

For many years, the N_2O laser has been secondary to the CO_2 laser as a source of coherent radiation in the 10- μm region. Although N_2O has twice as many laser lines as does CO_2 , spanning a comparable wavelength range, the N_2O laser is generally used only when the frequency coverage of the CO_2 laser is inadequate. Applications have been primarily as a secondary frequency standard,^{1,2} and in areas of spectroscopy.^{3,4} This situation has arisen because N_2O lasers have much lower small-signal gain and output powers than CO_2 lasers, despite similarities in molecular spectroscopy, laser design, and net line strength. Relatively speaking, the N_2O system has received little attention. Since the first observation of pulsed laser action in pure N_2O in late 1964,⁵ and the first achievement of continuous (cw) lasing in N_2O-N_2 in early 1965,⁶ most investigations have been concerned with observing new lines^{7,8} or making accurate frequency measurements^{9,10} of the (00^01-10^00) transitions. In 1977, lasing on the (00^02-10^01) sequence lines of N_2O was obtained¹¹ using an in-cavity hot cell to suppress lasing on the regular 10- μm transitions. Few attempts to examine gain dynamics have been made,¹² but it has been observed that, under similar conditions, the small signal gain of the CO_2 laser exceeds that of the N_2O laser by roughly a factor of four.¹³ This situation is

responsible for the lower efficiency and output power of the N_2O laser. Hitherto, the difference in the gains for the two systems has been attributed to dissociation of the N_2O molecule,^{11,14} which occurs more readily than for CO_2 . Although the mechanisms governing gain in the two molecules are similar, no systematic study of gain in N_2O exists to date.

To conclusively determine the factors limiting small-signal gain, and hence power, in the N_2O laser, a tunable diode laser (TDL) has been used to investigate the dynamics of cw N_2O discharges. The TDL possesses a distinct advantage over other laser sources in that it can be tuned to any vibrational transition in N_2O ; investigations are no longer limited to transitions that will lase in a separate N_2O oscillator. Whereas in the past, information concerning only the difference in the populations of the two laser levels was available,¹⁵ with this technique one can monitor the populations in all three normal vibrational modes of N_2O and determine the vibrational temperature associated with each mode. This thesis discusses the use of a TDL to study cw electric discharges in flowing gas mixtures of N_2O , N_2 and He. The measurements are similar to those of Dang et al.¹⁶ in their comprehensive examination of the gain dynamics of CO_2 , but the present investigation is particularly concerned with determining the factors which limit small-signal 10- μm gain in the N_2O laser.

The results indicate that the mode-temperature model of Gordietz et al.¹⁷ and Moore et al.¹⁸ provides a good description of the vibrational populations in an N_2O discharge. The model assumes independent vibrational modes whose populations follow a Boltzmann

distribution characterized by a vibrational temperature for each mode. The ν_1 and ν_2 modes are found to be strongly coupled and to have the same vibrational temperature. The ν_3 vibrational temperature is the most important factor influencing gain insofar as it governs the population in the upper laser level. Results clearly show that saturation of the ν_3 mode excitation is the primary factor limiting gain in N_2O discharges. A similar saturation has been observed in CO_2 discharges,^{15,16,19} but the effect is much more severe in N_2O . This factor results in significantly lower gain coefficients in N_2O lasers which, in turn, account for the poor performance of the N_2O laser relative to the CO_2 laser. In contrast to previous investigations of N_2O lasers,^{11,13} dissociation of N_2O is not found to be a major problem.

The next chapter presents theoretical background concerning the spectroscopy of N_2O , and energy transfer mechanisms within the system. The conventional mode-temperature model is reviewed, and the vibrational level populations are related to the absorption coefficients measured with the TDL. Chapter 3 outlines the experimental and analytical techniques for determining vibrational temperatures, while N_2O dissociation is examined in Chapter 4. In Chapters 5 and 6, results of temperature measurements as a function of discharge current and gas mixture are discussed with regard to the limitations on 10- μm gain in N_2O lasers. Conclusions are presented in the final section.

CHAPTER 2

THEORY

2.1 Introduction

This chapter briefly introduces the theory of small-signal gain and absorption on the regular 10- μm laser transitions and the 4.5- μm absorption transitions of the $\text{N}_2\text{O}:\text{N}_2:\text{He}$ system in an electric discharge. These concepts are necessary to an understanding of the methods of investigation and analysis used in this work. A discussion of the structure and spectroscopy of the N_2O molecule is followed by an outline of the principal mechanisms involved in the excitation of laser gas molecules, and in the establishment of population inversion. Subsequently, the theoretical mode-temperature model is presented, and is used in calculating the vibrational energy level populations in N_2O . These populations determine the magnitude of the gain or absorption on a transition. Once the theoretical results of the model have been shown to be in good agreement with experimental measurements, the model becomes a powerful tool in the study of factors governing small-signal gain in the N_2O laser.

Due to the similarities between the N_2O and CO_2 molecules, the following pages include occasional references to the CO_2 system, for which considerably more published material exists.

2.2 Spectroscopy of N₂O

The spectroscopy of a molecular gas is determined by the structure of the molecules and their normal mode vibrations. These factors, in combination with quantum mechanical selection rules, govern the frequency and intensity of electro-magnetic radiation absorbed or emitted by the gas.

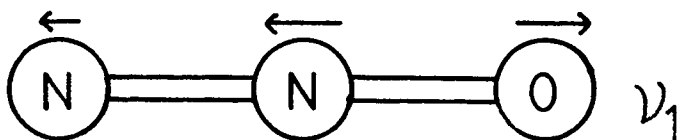
N₂O is a linear, asymmetric triatomic molecule with an axis of symmetry C_∞. There are four fundamental modes of vibration, two of which are degenerate. Figure 2.1 shows the three distinct modes of vibration and their frequencies. The ν₁ and ν₃ modes involve atom movement parallel to the axis, while ν₂ represents a doubly degenerate bend in two equivalent planes perpendicular to the molecular axis that connects the nuclei at rest. Energy stored in a molecule in the form of these vibrations can have only certain quantized values denoted by "ij^ℓk". The three vibrational quantum numbers i, j and k take on integer values designating the number of quanta of vibrational energy excited in each of the three vibrational modes. The ℓ quantum number specifies the vibrational angular momentum associated with the ν₂ bending mode.

The purely vibrational energy of a particular state ij^ℓk is calculated as:²⁰

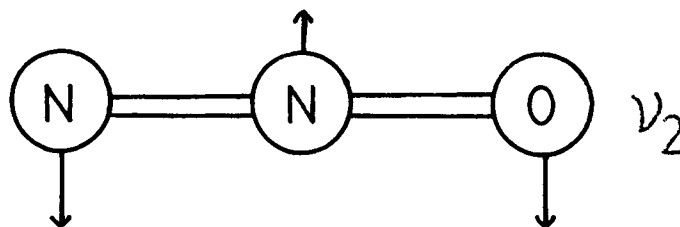
$$G(ij^{\ell}k) = \sum_{m=1}^3 \nu_m (v_m + d_m/2) + \sum_{m=1}^3 \sum_{n \geq m}^3 \chi_{mn} (v_m + d_m/2)(v_n + d_n/2) + \sum_{m=1}^3 \sum_{n \geq m}^3 g_{mn} \ell_m \ell_n, \quad (1)$$

FIGURE 2.1 The normal modes of vibration of the N_2O molecule. The vibrational frequencies and symmetry types (species) are also indicated.

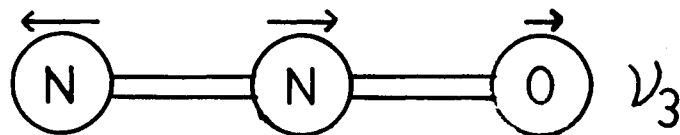
N=O stretch
 1285 cm^{-1}
 Σ^+



Doubly degenerate
bend
 588 cm^{-1}
 Π



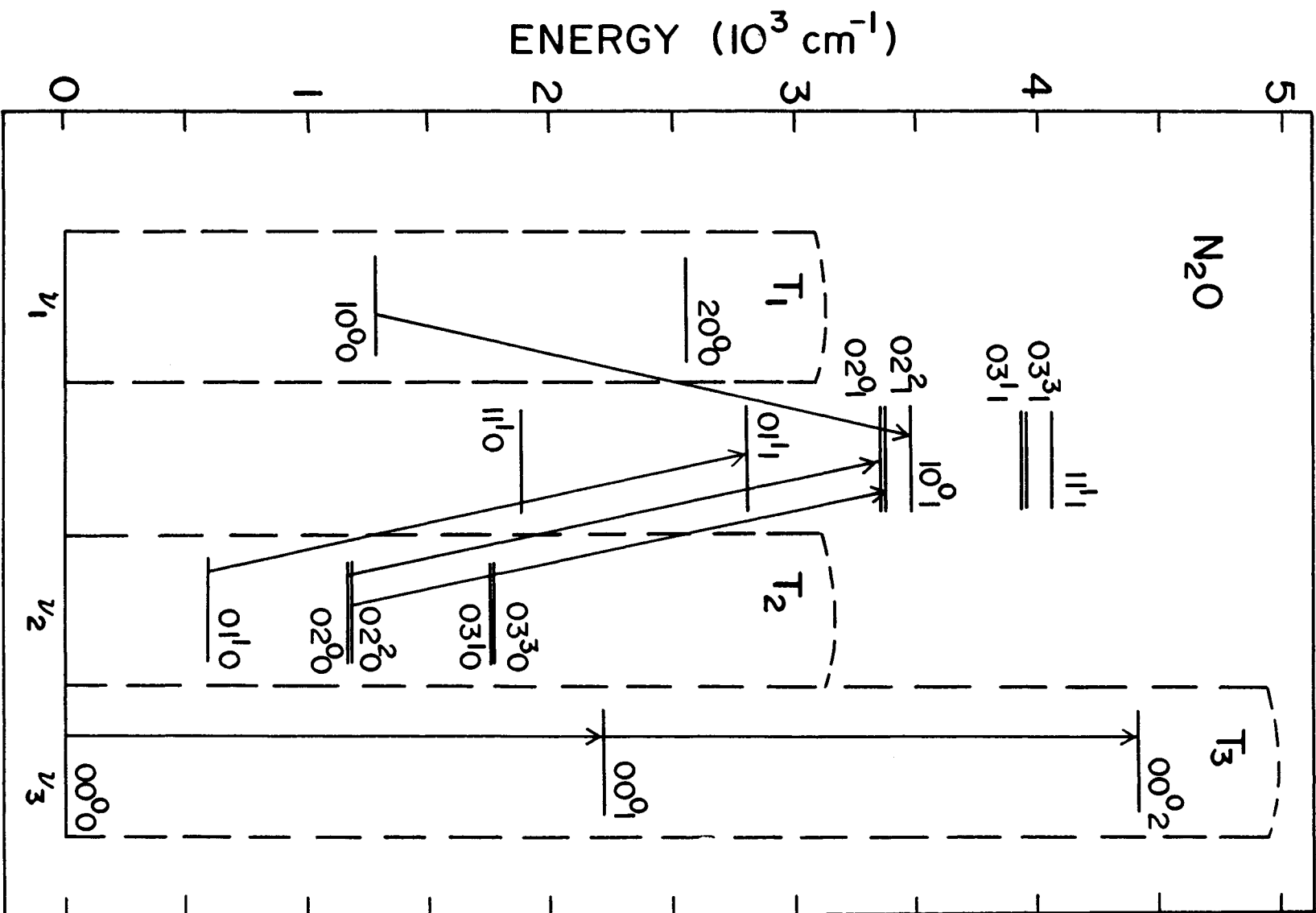
N=N stretch
 2223.8 cm^{-1}
 Σ^+



where v_m ($m=1-3$) are the quantum numbers i , j and k . The χ_{mn} represent a small amount of coupling between the fundamental modes due to anharmonicity. This arises because the vibrational displacements of the molecules are not infinitesimal, and leads to a slight decrease in the energy spacings of the modes with increasing quantum number. The g_{mn} are on the same order as χ_{mn} , and for non-degenerate vibrations $g_{mn}=0$, $\ell_{m,n}=0$, $d_m=1$. A doubly degenerate vibration has $d_m=2$. The experimentally observed values of the vibrational energy G are shown in the energy level diagram in Fig. 2.2.

In addition to molecular vibration, simultaneous rotation can also occur producing a rotational angular momentum designated by the quantum number J . This leads to an additional contribution to the energy of the molecule and causes a sub-structure of rotational levels to be superimposed on each vibrational level. The statistical weight of a rotational level is given by $g_J=2J+1$, the number of possible projections of J along a space-fixed axis. The rotational structure is further influenced by the ℓ -value mentioned above. A classical visualization of the vibrational contribution to the angular momentum of the molecule by the degenerate bending mode considers the two components of the ν_2 mode to be excited simultaneously, but out of phase with each other. As a result, each atom describes an ellipse (or circle) about the internuclear axis and since all the atoms do not move in phase, the molecule appears to be rotating in a slightly bent position. This produces a constant vibrational angular momentum quantized by ℓ , where $\ell=j, j-2, \dots -j$. The $\pm|\ell|$ values arise from the possibility of either

FIGURE 2.2 Partial vibrational energy level diagram for N_2O showing the three fundamental modes with their associated mode temperatures. Also shown are some typical transitions in the 2200 cm^{-1} region that are probed with the tunable diode laser.



clockwise or anti-clockwise rotation. Normally, the absolute value of ℓ is given in the notation $ij^{\ell}k$. The ℓ value determines the symmetry type or species of a vibrational mode, where $\ell=0,1,2,3\dots$ corresponds to species $\Sigma,\Pi,\Delta,\Phi\dots$. Consider the state 02^0_0 , for which $\ell = \pm 2, 0$. The effects of vibrational anharmonicity lead to a splitting of the 02^2_0 level from the 02^0_0 level, and a coupling of vibration to rotation by the Coriolis force causes levels for which ℓ is non-zero to be split into two new levels per J value. This is called ℓ -type doubling. Each rotational level is assigned a parity '+' or '-' depending upon whether or not the total eigenfunction of the molecule, including contributions from the electronic, vibrational and rotational eigenfunctions, changes sign when all particles are reflected at the origin (inversion). Furthermore, the two levels arising from ℓ -type doubling are labelled 'e' or 'f' according to the parity of the level and the J value.²¹ An increase in Coriolis force with increasing rotational energy causes the separation of the e and f levels to grow as the J number rises. These characteristics of the rotational structure of vibrational levels are depicted in Fig. 2.3.

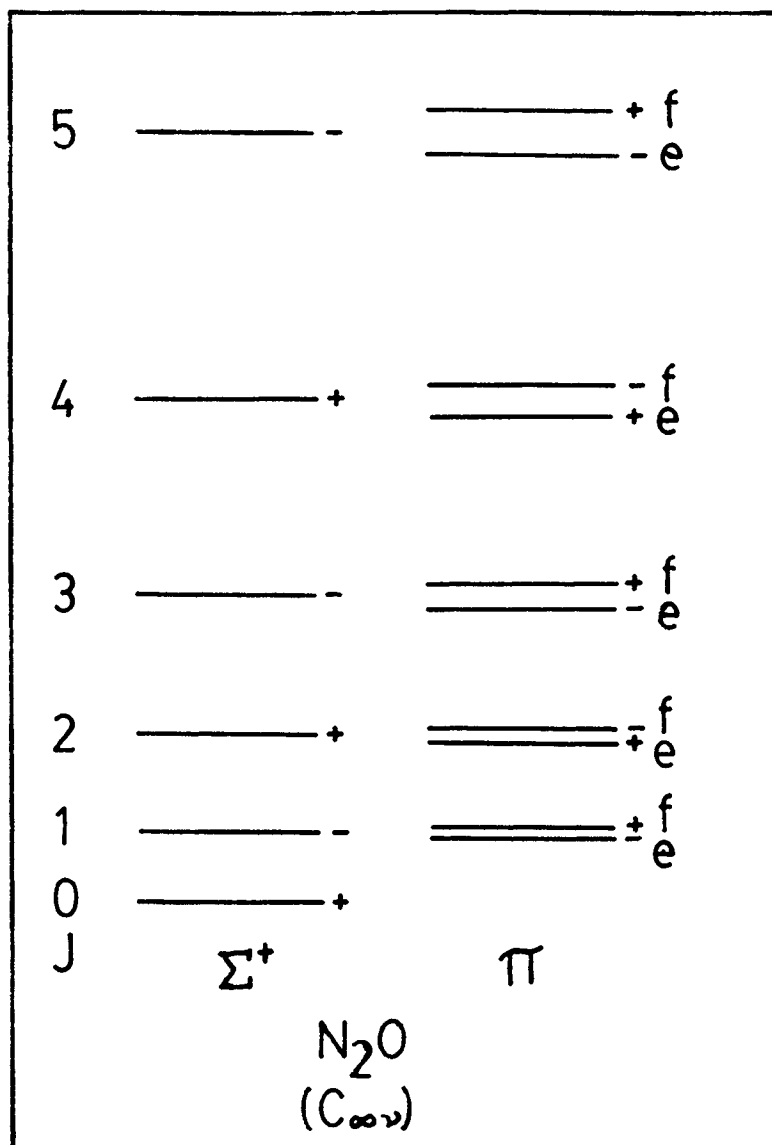
The net energy of a rotational-vibrational level is given by the sum of the vibrational energy $G(ij^{\ell}k)$ and the rotational energy $F(J)$:

$$E = G(ij^{\ell}k) + F(J) \quad (2)$$

$$F(J) = B[J(J+1)-\ell^2] - D[J(J+1)-\ell^2]^2 + H[J(J+1)-\ell^2]^3 + \dots \quad (3)$$

In all cases, $J > \ell$, which accounts for the absence of the $J=0$ level for species Π in Fig. 2.3. The dominant influence on the rotational energy

FIGURE 2.3 The rotational sub-structure superimposed upon the vibrational energy levels is shown for two different vibrational symmetry species, e.g., the 00^0_0 (Σ) and 01^1_0 (Π) modes.



is the rotational constant B , which varies inversely as the moment of inertia I of the molecule. B decreases slightly for each vibrational level of increasing energy, due to the corresponding increase in I . D represents the influence of centrifugal stretching introduced by the interaction of vibration and rotation, and both D and H are several orders of magnitude smaller than B . The spectroscopy of N_2O in the $4.5\text{-}\mu\text{m}$ region has been studied in considerable detail,²²⁻²⁶ and molecular constants for most of the levels of interest in this work are available in the literature. The frequency of a transition between two levels is simply given by the energy difference in cm^{-1} between the levels in question. Consequently, the majority of absorption lines observed with the TDL can easily be identified. All constants used in the frequency calculations are recorded in Table 2.1.

The selection rules influencing infrared transitions between rotational-vibrational levels are as follows:

1. Vibrational Transitions

$$\Delta \ell = 0, \pm 1; \quad \Sigma^+ \not\leftrightarrow \Sigma^-$$

2. Rotational Transitions

(4)

$$\Delta J = 0, \pm 1 \quad (J=0 \not\leftrightarrow J=0); \quad + \leftrightarrow -,$$

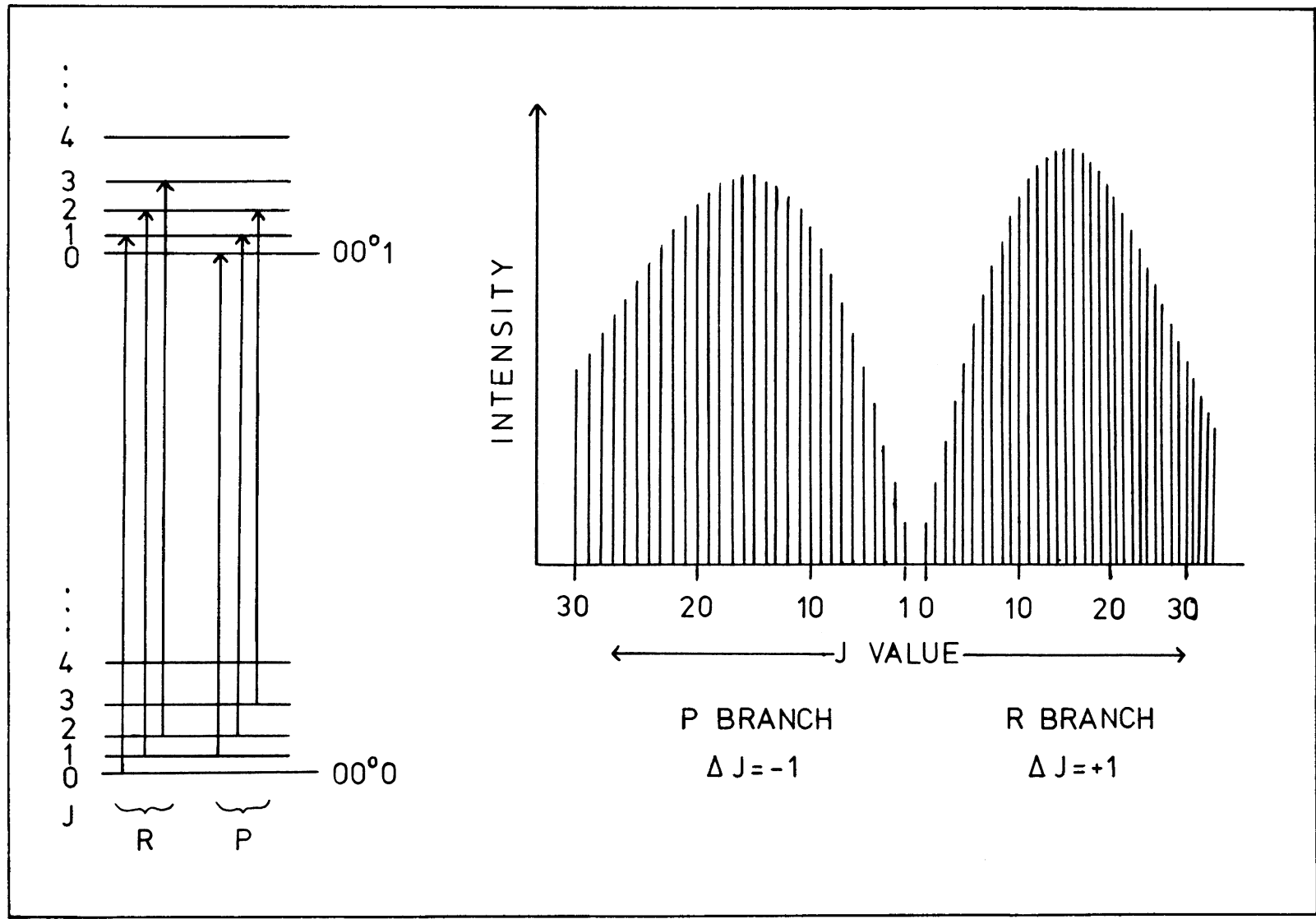
where \leftrightarrow and $\not\leftrightarrow$ mean 'allowed' and 'not allowed'. A rotational-vibrational spectrum typically consists of an R branch ($\Delta J = +1$) and a P branch ($\Delta J = -1$), as shown in Fig. 2.4. A spectral line is labelled by the J value of its lower level. The Q branch ($\Delta J = 0$) does not exist for transitions in which $\ell=0$ in both the upper

TABLE 2.1

Molecular Constants Used for N₂O Transition Frequency Calculations

Vib. Level	G(cm ⁻¹)	B(cm ⁻¹)	D(cm ⁻¹) ×10 ⁻⁷	H(cm ⁻¹) ×10 ⁻¹⁴	Iso- tope	Ref.
00 ⁰ 0	0	0.4190110	1.7618	0	446	24
"	0	0.4048586	1.637	0	546	23
"	0	0.4189825	1.7632	0	456	23
00 ⁰ 1	2223.757	0.415560	1.7585	3.8	446	24
"	2201.605	0.4014979	1.633	0	546	23
"	2177.658	0.4156541	1.7566	2.2	456	23
00 ⁰ 2	4417.382	0.4121007	1.7090	0	446	24
00 ⁰ 3	6580.856	0.4086376	1.754	0		25
00 ⁰ 4	8714.146	0.4051866	1.788	0		25
01 ¹ 0e	588.768	0.4191775	1.7852	0		24
" f	588.768	0.4199695	1.7922	0		24
01 ¹ 1e	2798.293	0.4157703	1.7771	0		24
" f	2798.293	0.4165475	1.7868	1.4		24
01 ¹ 2e	4977.695	0.4123583	1.785	117		22
" f	4977.695	0.4131183	1.785	117		22
02 ⁰ 0	1168.134	0.4199193	2.445	117		22
02 ⁰ 1	3363.974	0.4165443	2.445	117		22
02 ² 0e	1177.750	0.4201253	1.165	117		22
" f	1177.750	0.4201253	1.795	117		22
02 ² 1e	3373.137	0.4167523	1.195	117		22
" f	3373.137	0.4167523	1.795	117		22
03 ¹ 0e	1749.058	0.4196063	2.195	117		22
" f	1749.058	0.4210883	2.195	117		22
03 ¹ 1e	3931.258	0.4162253	1.915	117		22
" f	3931.258	0.4176843	1.925	117		22
03 ³ 0e	1766.958	0.420674	1.805	14		26
" f	1766.958	0.420674	1.805	220		26
03 ³ 1e	3948.344	0.417327	1.815	14		26
" f	3948.344	0.417327	1.815	220		26
10 ⁰ 0	1284.907	0.4172563	1.775	117		22
10 ⁰ 1	3480.821	0.4137843	1.745	117		22
11 ¹ 0e	1880.268	0.4174673	1.765	117		22
" f	1880.268	0.4183803	1.775	117		22
11 ¹ 1e	4061.979	0.4140513	1.775	117		22
" f	4061.979	0.4149343	1.735	117		22

FIGURE 2.4 Typical rotational-vibrational spectrum showing the P and R branches of the fundamental band ($00^0_1-00^0_0$). Transitions between vibrational levels also involve a change in rotational quantum number J . The spectral transitions are labelled by the J value of the lower level, e.g., $00^0_0 J=4 \rightarrow 00^0_1 J=5$ produces the R(4) line.



and lower states, and is weak for transitions in which $\Delta l = 0$, but $l \neq 0$. Both cases are called parallel band transitions, and in this thesis absorption measurements are made on particular rotational lines of these parallel bands. Perpendicular bands correspond to $\Delta l = \pm 1$.

In passing, it should be mentioned that the similarities in the structures of CO_2 and N_2O cause their spectra to closely resemble one another, with the exception that for CO_2 alternate J lines are missing. This difference accounts for the interest in N_2O for more complete spectral coverage of the 10- μm region.

2.3 Excitation and Energy Transfer Mechanisms

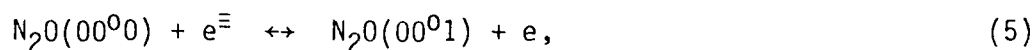
The simplest and most popular technique conventionally used for the excitation of N_2O laser gases employs a continuous (cw) electric discharge. As this thesis is concerned with the gain behaviour in cw lasers, the following paragraphs review the mechanisms operating in a discharge to populate the upper laser level and empty the lower. For successful laser action, a population inversion between the laser levels must be maintained. The magnitude of the inversion is governed by the energy exchange rates between the various levels. Furthermore, the assumptions incorporated into the theoretical model that is presented in Section 2.4 are justified by the following picture of energy transfer within the $\text{N}_2\text{O}:\text{N}_2:\text{He}$ system. Note that, for this study, it is primarily the relative rates for intramode and intermode energy exchange that are of interest.

2.3.1 Excitation of $N_2O(00^01)$

In a laser-gas discharge, electron energy is transferred by means of collisions into translational, vibrational and rotational motion of the gas components. Electronic excitation of the molecules and atoms, as well as ionization and dissociation, also occur. A detailed theoretical calculation of the transfer of input power to the vibrational modes of the constituent gas molecules requires knowledge of such quantities as the electron density and energy distribution, and collision cross-sections between all components. Although calculations have been done for the CO_2 laser,^{27,28} many of the necessary rate constants and collision cross-sections have not been measured for N_2O . However, the similarities between the N_2O and CO_2 molecular systems suggest that many of the mechanisms operating in CO_2 will also apply to N_2O .

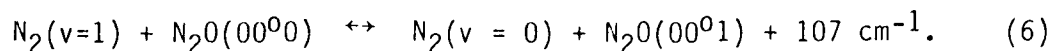
Excitation of the upper laser level (00^01) of N_2O is accomplished by two processes:

(1) Direct electron excitation of N_2O



where $e^{\bar{}}$ indicates an energetic electron.

(2) Direct excitation of the nitrogen and subsequent vibrational-to-vibrational (V-V) energy transfer from the first excited state of N_2 at 2330.7 cm^{-1} to N_2O at 2223.7 cm^{-1} ,



Nitrogen molecules have been shown to have a large cross-section for

vibrational excitation by direct electron impact.²⁹ Furthermore, the vibrational energy difference between the N_2 and N_2O levels is less than kT ,³⁰ and thus the probability of vibrational energy transfer is high. Fast coupling rates between excited nitrogen and $N_2O(00^01)$, on the order of $5.6 \times 10^3 \text{ s}^{-1}\text{Torr}^{-1}$, ensure that the ν_3 mode of N_2O and the excited N_2 are in equilibrium with one another.³¹⁻³³ A similar equilibrium between CO_2 and N_2 has been observed in CO_2 mixtures, where the ν_3 -mode excitation is very dependent upon the relative proportions of N_2 and CO_2 in a laser gas.^{19,34} Since the 10^00 lower laser level of N_2O at 1285 cm^{-1} is removed by 1046 cm^{-1} from the $N_2(v=1)$ level, little energy transfer occurs between these two levels. Consequently, selective excitation of the upper laser level is achieved.

2.3.2 Relaxation Processes

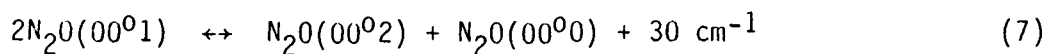
In the cw N_2O laser, discharge excitation establishes a population in the upper laser level, as well as in the low-lying ν_1 and ν_2 vibrational modes of N_2O . During lasing, population is transferred from the 00^01 to the 10^00 level, and the return to ground state proceeds via the 020 and 010 levels. Simultaneously, other mechanisms may act to remove molecules from the upper laser level. In order that population inversion be maintained, energy transfer rates must be such that a 'bottle-neck' of population does not occur in any of the relevant levels. The processes by which energy is re-distributed in the system are outlined below.

In cw electric discharges, there are four principal routes by which population can be removed from excited levels to the ground state.

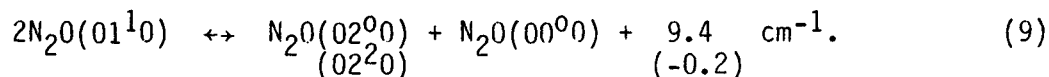
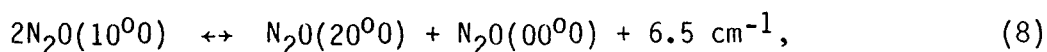
Collisional relaxation processes, which are dominant in the discharges of this study, will be discussed in detail. Conversely, diffusion to the walls becomes significant only at very low pressures, and spontaneous emission rates, which are on the order of seconds to milliseconds,^{32,33,35} are negligible in comparison to other processes. Electron de-excitation of vibrationally excited molecules has been shown to have a profound effect upon CO₂ discharges, and to dominate other relaxation processes for high electric discharge currents.³⁶ The effects of electron de-excitation in N₂O have been observed in this work and are presented in Chapter 5.

Of the possible collisional relaxation processes, rotational relaxation is the fastest. Measurements³⁷⁻⁴⁰ show that rotational coupling in the N₂O molecule is practically identical to that for CO₂, which has a relaxation rate on the order of $10^7 \text{ s}^{-1}\text{Torr}^{-1}$. Corresponding rates for N₂ and He are $k_R(\text{N}_2) = 1.2 \times 10^7 \text{ s}^{-1}\text{Torr}^{-1}$ and $k_R(\text{He}) = 0.6 \times 10^7 \text{ s}^{-1}\text{Torr}^{-1}$.³⁹ These rates ensure that the rotational sub-levels of a vibrational level will be thermalized.

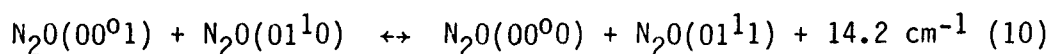
Resonant V-V exchange processes during N₂O-N₂O collisions account for the distribution of energy throughout a single mode. In CO₂, the intramode exchange rates are much faster than the intermode and vibrational-translational (V-T) transfer rates. In N₂O also, the ν_3 intramode exchange rate is one of the fastest V-V rates known.⁴¹ This a consequence of the small vibrational energy differences between the states of the molecules in comparison to the translational energy,³² and of the large transition dipole moments involved in the collisions of molecules of the same kind.⁴¹ In the case of N₂O, reactions of the form



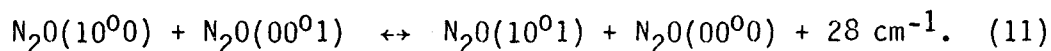
are sufficiently rapid to establish a vibrational equilibrium in the repartition of the populations of the ν_3 mode. Similar energy exchange within the $N=0$ stretch mode and the bending mode is expected to occur as follows:



In addition, transfer between the 02^00 and 02^20 states takes place. Pack⁴² suggests that calculated rates at 400 K for the equivalent of equation (7) in CO_2 are on the order of $1 \times 10^7 \text{ s}^{-1}\text{Torr}^{-1}$. Although measurements of this rate are unavailable for N_2O , the rate constant is expected to be larger than those for similar processes of the form:



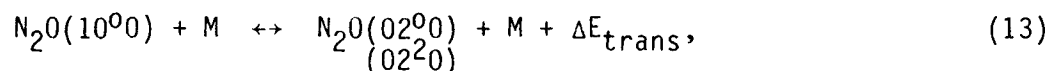
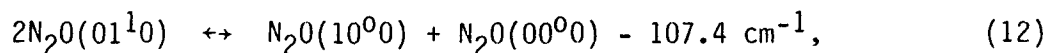
and



Measured rates for both of these cases are $1.6 \times 10^6 \text{ s}^{-1}\text{Torr}^{-1}$. It can therefore be concluded that vibrational equilibrium within the levels of each of the three normal modes of N_2O is established very rapidly.

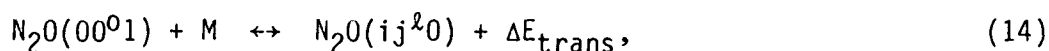
Re-distribution of energy within the N_2O system also occurs through intermode resonant V-V transfers involving the ν_1 and ν_2 modes.

The following processes control the relaxation of the lower laser level, and thus influence the population inversion:



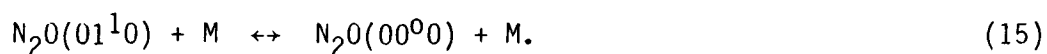
where ΔE_{trans} is the excess energy that goes into translational motion and M is any of the constituent gas molecules. Although specific rates for these reactions could not be found in the literature, the equilibrium⁴³ observed between the two modes indicates that V-V coupling is very rapid. Henceforth this 'joint mode' will be designated (ν_1, ν_2). Experimental evidence for this coupling is presented in Chapter 4.

In contrast to the energy transfer processes already outlined, intermode exchange between the N_2O ν_3 and (ν_1, ν_2) modes is quite slow. The reaction is written



and is temperature dependent. In pure N_2O at 300 K, the de-excitation rate of the 00^0_1 level is $\sim 750 \text{ s}^{-1}\text{Torr}^{-1}$,^{35,44} while for N_2O in He the rate is $260 \text{ s}^{-1}\text{Torr}^{-1}$. It is believed that the principal path for de-excitation of the $\text{N}_2\text{O}(00^0_1)$ level by rare gases is through the 11^1_0 level. Relaxation of $\text{N}_2\text{O}(00^0_1)$ by N_2 at 400 K proceeds at $460 \text{ s}^{-1}\text{Torr}^{-1}$.³²

Finally, the relaxation of the lower level (ν_1, ν_2) modes is assisted by helium through vibrational-to-translational (V-T) processes such as



Helium is commonly used as a buffer gas in laser gas mixtures due to its high thermal conductivity, which lowers the gas temperature and allows higher pumping currents to be used.⁴⁵ De-excitation of (ν_1, ν_2) can also occur by collisions with N_2O and N_2 . Measured relaxation rates are $2950 \text{ s}^{-1}\text{Torr}^{-1}$ and $1770 \text{ s}^{-1}\text{Torr}^{-1}$, respectively.³¹

To summarize the preceding paragraphs, it is found that in the discharges examined in this work, rotational relaxation proceeds more rapidly than other processes. Thus, an equilibrium Boltzmann distribution is established in the rotational sub-levels of each vibrational level. Furthermore, intramode V-V energy exchange rates dominate intermode and V-T rates such that the N_2O vibrational modes can be considered as distinct. These points justify the assumptions upon which the theoretical mode temperature model of the following section rests.

2.4 The Mode-Temperature Model

The theoretical mode-temperature model for populations in molecular energy levels was first introduced by Gordietz et al.¹⁷ and Moore et al.,¹⁸ and has been used by several workers for investigations of CO_2 lasers.^{15,16,19,36,46} The spectroscopy and laser dynamics of the N_2O and CO_2 systems are sufficiently similar that the theory can be applied to N_2O with only minor alterations.

The model assumes that the vibrational level populations of each

mode of N_2O are characterized by a Boltzmann distribution. Thus, vibrational temperatures T_1 , T_2 and T_3 are associated with modes ν_1 , ν_2 and ν_3 , respectively. For simplicity, exponential factors x_1 , x_2 and x_3 are introduced, such that

$$x_n = \exp(-h\nu_n/kT_n), \quad (16)$$

where $h\nu_n$ is the level spacing of the n^{th} mode. Planck's constant h and Boltzmann's constant k appear in the exponential factor. The successful application of the model to cw and pulsed CO_2 lasers is attributed to very rapid CO_2 intramode relaxation rates.⁴² A similar situation is expected to hold for N_2O , as discussed in the previous section. Good agreement between results produced by this model and experimental measurements reported in Chapters 3 and 5 adds further support to the theoretical approach. A fourth temperature T is defined to describe the distribution of the population of a vibrational level through the rotational sub-levels. As mentioned in Section 2.3, the rotational relaxation rates in $N_2O:N_2:He$ mixtures are sufficiently rapid that the rotational temperature is assumed equal to the translational gas temperature.

In this work, a TDL operating in the 2120-2350 cm^{-1} region is used to measure absorption coefficients in the fundamental ν_3 band of N_2O , and all of its associated hot bands. Thus transitions between levels (ij^k) and (ij^{k+1}) are monitored. Typical transitions are shown in Fig. 2.2. From the absorption coefficients of such transitions, the population difference $[N(ij^k) - N(ij^{k+1})]$ can be deduced. The relationship between these population differences and the absorption

coefficients has been derived for the 4.3- μm bands of CO_2 by Dang et al.¹⁶ A similar approach is adopted here, modified as appropriate for the 4.5- μm bands of N_2O .

The population density in a particular vibrational level (ij^lk) is written

$$\begin{aligned} N(ij^lk) &= \frac{N_0}{Q_v} g_v \exp[-G(ij^lk)/kT] \\ &= \frac{N_0}{Q_v} g_i g_j g_k x_1^i x_2^j x_3^k, \end{aligned} \quad (17)$$

where N_0 is the density of N_2O molecules, g_v indicates the degeneracy of the vibrational levels, and Q_v is the vibrational partition function given by

$$Q_v = (1 - x_1)^{-1} (1 - x_2)^{-2} (1 - x_3)^{-1}. \quad (18)$$

To obtain the population density of an individual rotational sub-level, $N(ij^lk)$ is multiplied by the Boltzmann rotational population factor $K(J)$:

$$n(ij^lk;J) = K(J) N(ij^lk), \quad (19)$$

$$K(J) = \frac{g_J}{Q_R} \exp[-F(J)/kT]. \quad (20)$$

Generally in the calculation of the exponential in F , it is sufficient to keep only the first order term in J , i.e., $F(J) = \exp[BJ(J+1)/kT]$. The statistical weight of the rotational level is $g_J = 2J+1$ (see Section 2.2)

and B is the molecular rotational constant. The rotational partition function Q_R is expressed as a summation over J ,

$$\begin{aligned} Q_R &= \sum g_J \exp[-F(J)/kT] \\ &= \sum (2J + 1) \exp[-BJ(J + 1)/kT]. \end{aligned} \quad (21)$$

Transforming the sum to an integral over all J -lines gives

$$\begin{aligned} \ell = 0 & \quad Q_R = kT/Bhc \\ \ell \neq 0 & \quad Q_R = 2kT/Bhc, \end{aligned} \quad (22)$$

where c is the speed of light.

2.5 Calculation of the Absorption Coefficient

The absorption of a photon by a molecular gas causes a transition between two energy levels of the gas. The absorption coefficient of the transition depends explicitly upon the population difference between the levels, as given by the expressions of the preceding section. Note that small-signal absorption is considered, implying that the radiation field intensities are sufficiently low that effects non-linear in the field need not be considered. Such an approximation is valid for the low diode laser probe powers involved in this work.

The absorption coefficient between an upper (u) and a lower (ℓ) level of a gas is expressed as⁴⁷

$$\alpha(\nu) = \frac{\lambda_0^2}{8\pi} A_{\ell}^u [K_{\ell} N_{\ell} (g_u/g_{\ell}) - K_u N_u] g(\nu), \quad (23)$$

where λ_0 is the wavelength at line centre, and g_u and g_{ℓ} are the rotational statistical weights of the respective levels. $g(\nu)$ is the normalized lineshape function. The spontaneous transition probability A_{ℓ}^u is given by

$$A_{\ell}^u = \frac{64\pi^4}{3h\lambda_0^3} \frac{|R_{\ell}^u|^2 S_J F_J}{g_u}. \quad (24)$$

The matrix element $|R_{\ell}^u|^2$ represents the vibrational contribution to the transition moment, while S_J is the rotational contribution and F_J is the interaction factor between vibration and rotation. Matrix elements for the fundamental (00⁰1-00⁰0) transition and the (00⁰1-10⁰0) laser transition have been measured,^{48,49} while values for other absorption lines are deduced using the harmonic oscillator approximation.⁵⁰ These constants are listed in Table 2.2, and expressions for S_J ⁵¹ are presented in Table 2.3. Measurements of F_J for the 4.5- μm transitions could not be found in the literature, but results for the N₂O 10- μm transitions⁴⁹ and in CO₂⁵² indicate that F_J is approximately unity. F_J values used in the calculations are included in Table 2.3.

The pressure regime required for the cw molecular gas discharges of this thesis dictate that the absorption lineshape will consist of a Doppler-broadened distribution of Lorentzian (pressure-broadened) profiles. Such a distribution is termed a Voigt profile,⁵³ and is used for the lineshape function $g(\nu)$ in expression (23). Only the absorption

TABLE 2.2

Vibrational Matrix Elements and F_J Values for N_2O

Transition		$ R_\ell^u $	F_J
4.5 μm	00^0_0	0.249 Debye (a)	1 ↓
	00^0_1	$\sqrt{2}(0.249)$ (b)	
	00^0_2	$\sqrt{3}(0.249)$	
	00^0_3	$2(0.249)$	
	01^1_0 e,f	$(0.249)/\sqrt{2}$	
	01^1_1 e,f	0.249	
	02^0_0	0.249	
	02^2_0 e,f	$(0.249)/\sqrt{2}$	
	10^0_0	0.249	
	03^1_0 e,f	$(0.249)/\sqrt{2}$	
	03^3_0 e,f	$(0.249)/\sqrt{2}$	
	11^1_0 e,f	$(0.249)/\sqrt{2}$	
	10 μm	$00^0_1-10^0_0$	

(a) Kagann Ref. 48

(b) Harmonic oscillator approximation

(c) Lacombe et al. Ref. 49

TABLE 2.3

Expressions for S_J , the Rotational Contribution
to the Spontaneous Transition Probability

	P-branch $J_u = J_\ell - 1$	Q-branch $J_u = J_\ell$	R-branch $J_u = J_\ell + 1$
$\ell = 0$	J_ℓ	0	J_u
$\ell \neq 0$	$\frac{2(J_\ell^2 - \ell^2)}{J_\ell}$	$\frac{2(2J_u + 1)\ell^2}{J_u(J_u + 1)}$	$\frac{2(J_u - \ell^2)}{J_u}$

From Penner (51)

at line centre ν_0 is required in the present work, for which

$$g(\nu_0) = \frac{1}{\pi^{1/2} \gamma_C} b \exp(b^2) \operatorname{erfc}(b), \quad (25)$$

and erfc is the complementary error function. γ_C is the pressure-broadened halfwidth at half maximum (HWHM) and

$$b = (\gamma_C/\gamma_D) (\ln 2)^{1/2}. \quad (26)$$

The Doppler-broadened HWHM takes the form

$$\gamma_D = \nu_0 [(2kT \ln 2)/(Mc^2)]^{1/2} \quad (27)$$

and M is the mass of the molecules of the gas. Pressure broadening by N_2O , N_2 and He is given by⁵⁴

$$\gamma_C = \left(\frac{P}{760}\right) (\psi_{N_2O} c_{N_2O} + \psi_{N_2} c_{N_2} + \psi_{He} c_{He}) \left(\frac{T}{300}\right)^x, \quad (28)$$

where P is the total pressure, ψ_a is the fraction of gas 'a' in the mixture, c_a is the pressure-broadening coefficient of gas 'a', and T is the background gas temperature. N_2O self-broadening and N_2O - N_2 broadening coefficients are taken from Lacombe et al.,⁵⁵ while the temperature dependence of the broadening coefficients and the N_2O -He broadening are both assumed to be identical to the values measured in CO_2 mixtures by Brimacombe et al.⁵⁴ The J -dependence of these expressions is given in Table 2.4. The same linewidths are used for all the vibrational bands of interest in N_2O . The Doppler-broadened linewidth for N_2O at room temperature is $\psi_D(4.5 \mu m) \approx 60$ MHz, and

TABLE 2.4

Collision-Broadening Coefficients for N₂O

Collision Partners	m-Dependence of Coefficient
N ₂ O-N ₂ O	m ≤ 40 c _{N₂O} = 0.13 m ^{-0.118} (a)
	m > 40 c _{N₂O} = 0.121 - 6.86x10 ⁻⁴ m (a)
N ₂ -N ₂ O	all m c _{N₂} = 0.088 m ^{-4.92x10⁻³} (a)
He-N ₂ O	0 < m < 100 c _{He} = 5.98x10 ² - 2.8x10 ⁻⁵ m (b)

(a) Lacombe et al. Ref. 55

(b) Brimacombe & Reid Ref.54

Note: P-branch m=-J
R-branch m=J+1

$\psi_D(10 \mu\text{m}) \approx 26 \text{ MHz}$, while total linewidths are on the order of 30-40 MHz.

The preceding equations have been incorporated into a computer program which calculates the frequencies and absorption coefficients on any transition of interest as a function of gas mixture, pressure, and mode temperatures. Alternatively, the program can convert a measured absorption into a rotational or vibrational population difference. As described in the next section, TDL absorption measurements can thus be used to determine vibrational populations and mode temperatures.

The mode temperature model also allows calculation of laser gain, which occurs when a population inversion is present between two levels. It is noteworthy that 10- μm gain coefficients determined for both N_2O and CO_2 under identical conditions are very similar; the differences in experimentally determined gain coefficients cannot be predicted on the basis of the theoretical considerations outlined in this chapter. Hence, a systematic study of vibrational populations and mode temperatures under a variety of conditions is required to determine factors limiting N_2O laser gain.

2.6 Summary

The previous sections have presented the theory behind absorption and emission of photons in a molecular gas. The discussion of N_2O spectroscopy dealt with the origins of spectral lines and the means by which their frequencies are calculated, in order that they can be identified and measured. The excitation and energy transfer

mechanisms in a gas discharge have been outlined and assumptions based on the rates of energy exchange between molecules have been incorporated into a theoretical model for calculating populations of energy levels in N_2O . In addition, the relationship between populations and absorption or gain coefficients has been discussed. The next chapter deals with experimental procedure and data analysis techniques.

CHAPTER 3

EXPERIMENTAL APPARATUS AND MEASUREMENT TECHNIQUES

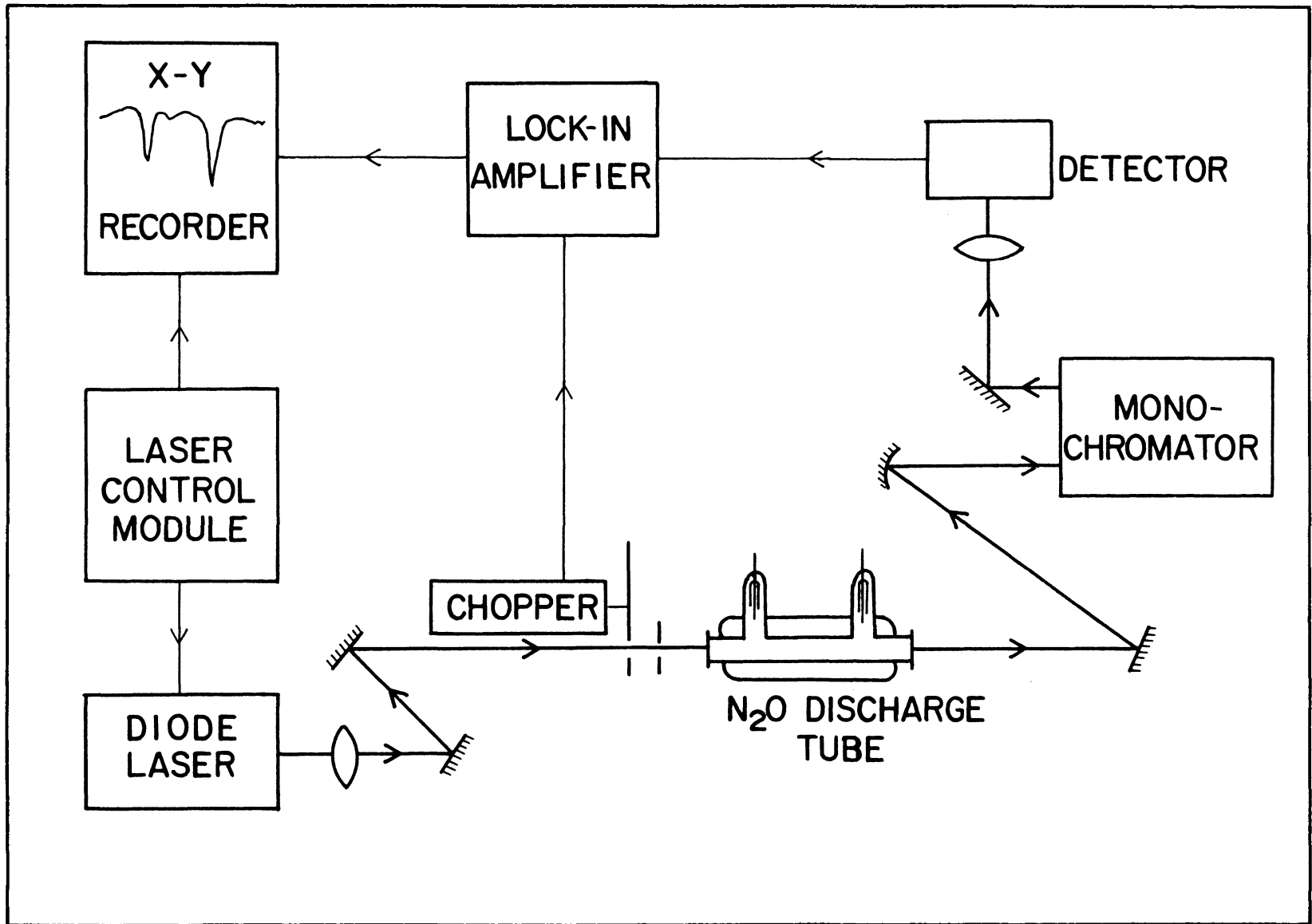
3.1 The Experimental System

A schematic diagram of the apparatus is shown in Fig. 3.1. The beam from a lead-salt tunable diode laser (TDL) is focussed into a short N_2O discharge tube, and imaged onto the slit of a 0.5 m monochromator. The radiation is subsequently collected at a HgCdTe detector and an X-Y recorder produces a trace of detected laser power versus diode laser frequency.

The TDL is mounted in an evacuated chamber (Laser Analytics, Inc.) and cooled by a CTI Cryogenic refrigerator to operating temperatures between roughly 10 and 50 K. Temperature adjustment and current tuning permit lasing at frequencies from $\sim 2120 \text{ cm}^{-1}$ to 2350 cm^{-1} . For ease in alignment of the infrared beam, a HeNe laser beam is arranged to traverse the same path as the TDL radiation. In general, several TDL modes lase simultaneously. The monochromator is used to isolate a single mode and allows coarse frequency calibration. Glass slides placed at the output of the diode laser attenuate the signals to levels below the saturation limit of the detector. These attenuators also reduce feedback into the laser from reflecting elements in the system.

The N_2O discharge tube has a bore of 1 cm, an active length of

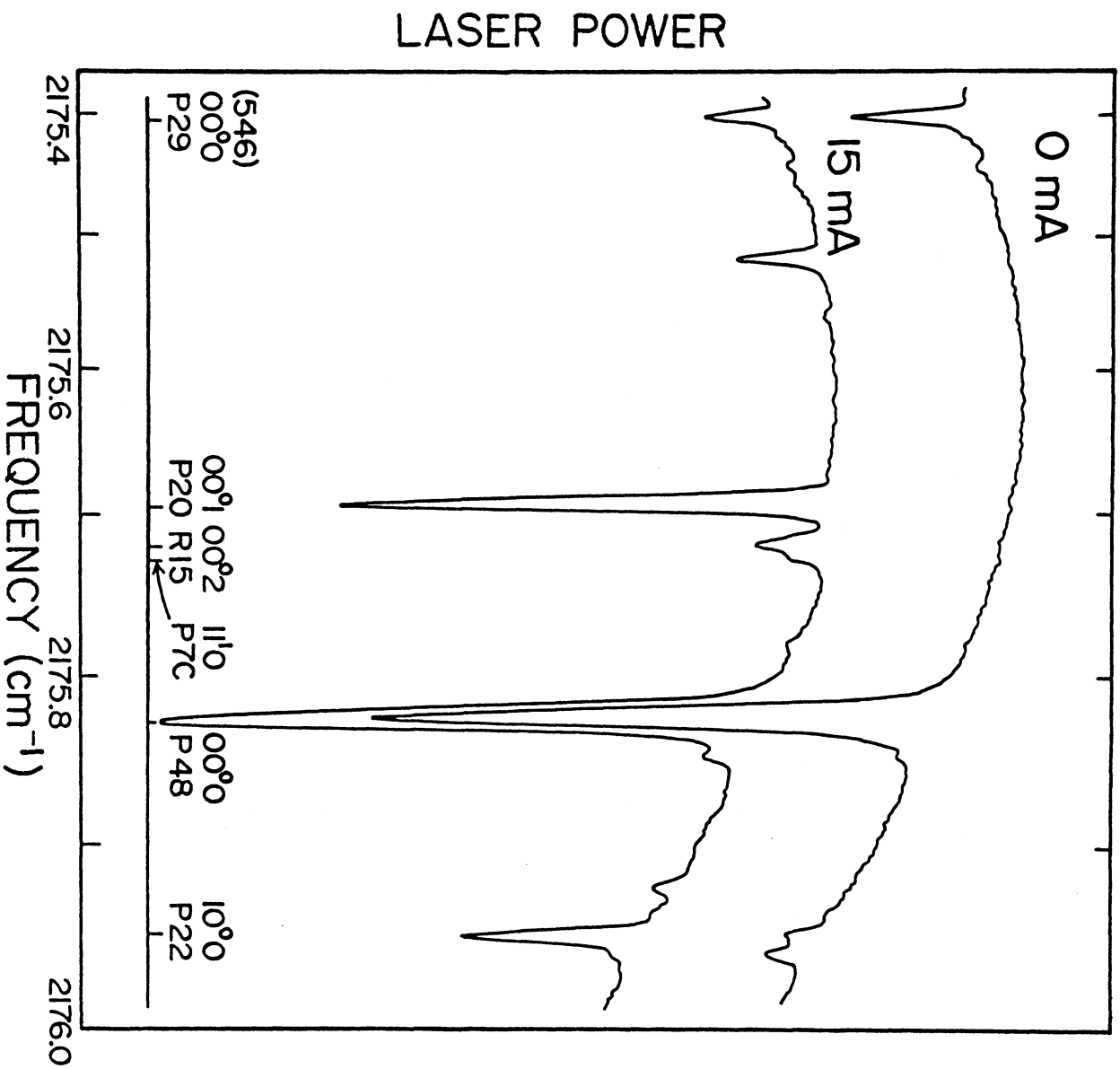
FIGURE 3.1 Schematic diagram of the experimental apparatus.



10 cm, and a total window-to-window length of 14.85 cm. Before entering the tube, the TDL beam diameter is restricted to ~ 3 mm by an aperture such that only the central portion of the discharge is probed. The discharge is operated with a Universal Voltronics Corporation high voltage power supply at typical voltages of ~ 2 kV and currents up to 25 mA. Fast gas flowrates of ~ 800 mL/min NTP are used to minimize dissociation, and the gas mixture is regulated using calibrated flowmeters. Gas pressures are measured with a calibrated pressure gauge at the outlet of the cell, and the pressure drop between inlet and outlet is found to be negligible. The methanol cooling jacket temperature is maintained at ~ 260 K.

Figure 3.2 shows two typical TDL absorption scans recorded with the laser beam passing through the discharge cell. These are conventional amplitude scans produced by mechanically chopping the infrared beam and using a lock-in amplifier with a liquid-nitrogen-cooled HgCdTe detector to achieve phase-sensitive detection. The absorption coefficients of lines examined in this work are sufficiently large (>0.2 %/cm) that high sensitivity harmonic detection techniques⁵⁶ are not required. Most of the lines can easily be identified using the theory presented in Section 2.2. The lower and upper traces of Fig. 3.2 are taken with and without a discharge current. Note the appearance of many additional absorption lines in the lower spectrum as the discharge populates high-lying vibrational levels. The strength of absorptions in the 00^0_1 and 00^0_2 bands⁵⁷ is indicative of the efficiency of excitation of the ν_3 mode of N_2O , and demonstrates the ability of the TDL technique to supply detailed information regarding

FIGURE 3.2 Typical TDL scans recorded with the laser beam focussed into the discharge tube. The upper scan is taken with no discharge current, while the lower scan corresponds to a current of 15 mA in a 15%N₂O:15%N₂:70%He mixture at 13.7 Torr. The more important absorption lines are labelled beneath the traces. Bracketed numbers indicate isotopes other than the most abundant ¹⁴N¹⁴N¹⁶O isotope, .e.g., ¹⁵N¹⁴N¹⁶O is labelled (546). Each transition is identified by its lower vibrational level.⁵⁷



population distributions in a discharge.

3.2 Mode Temperature Determination and Initial Results

As a first step in analyzing TDL traces such as those shown in Fig. 3.2, the upper non-discharge trace is considered. Since the absorption path-length ℓ is accurately known, the absorption coefficient $\alpha(\text{cm}^{-1})$ of a line can be determined using

$$I = I_0 \exp(-\alpha\ell), \quad (29)$$

where I and I_0 are the detected TDL beam intensities on and off resonance respectively. In the absence of a discharge, the N_2O molecules are in thermal equilibrium at a known temperature, pressure and gas mixture. Hence the measured absorption coefficients can be compared with those predicted by the model of Section 2.5. This comparison provides an experimental check on the matrix elements and linewidths for the various bands and in addition ensures that no systematic errors are present in the determination of gas mixture and pressure. In general, experiment and calculation agree to better than 7% for low-lying bands that can be monitored in a room temperature mixture.

The analysis procedure next requires that several suitable absorption lines be chosen for each vibrational band under investigation. The selected transitions must be free from interference by neighbouring lines; where possible, lines with J values near 19 are used to minimize the effects of varying gas temperature. Very large

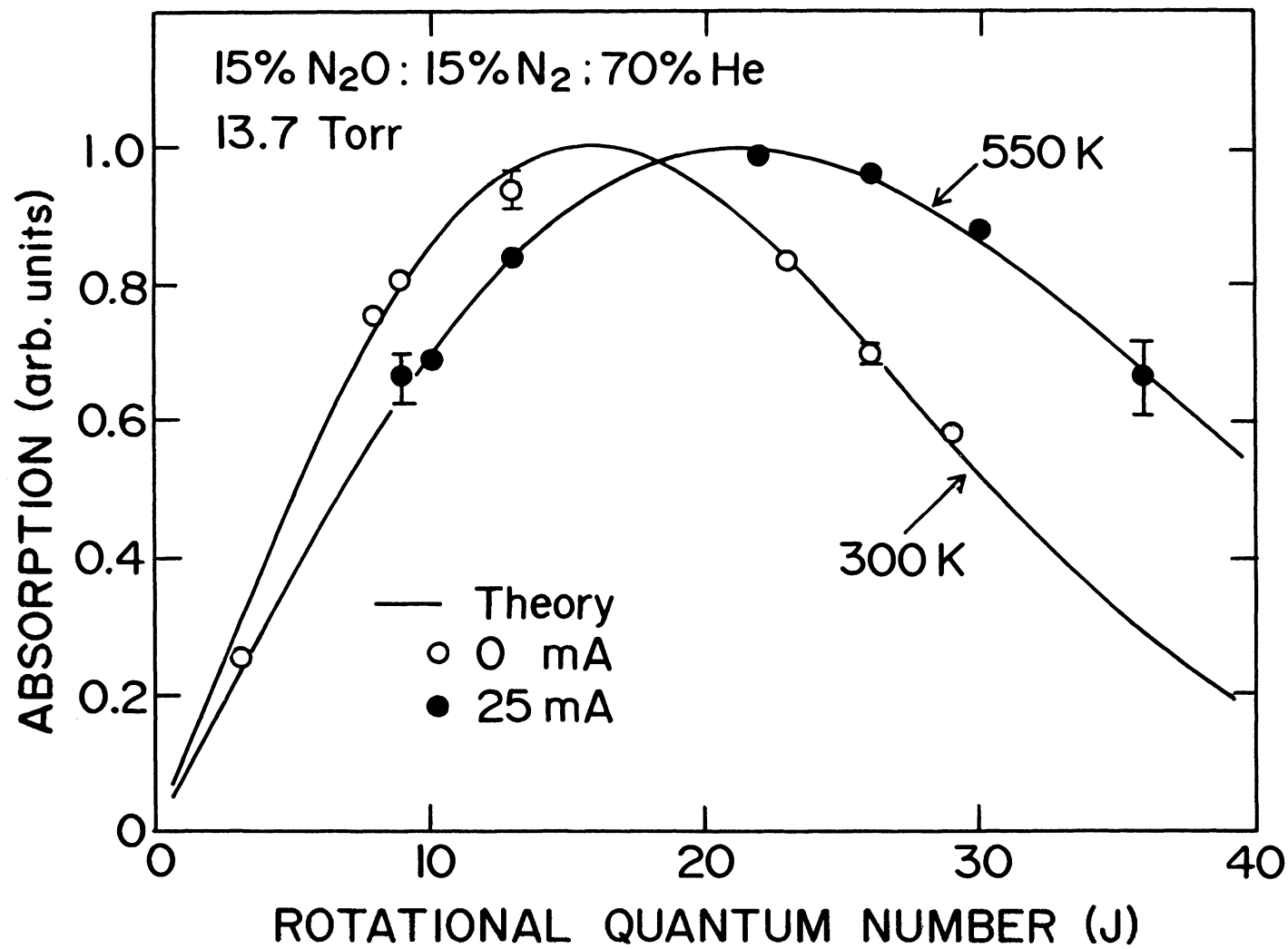
absorption coefficients in some spectral bands prohibit measurements at the branch peak, forcing examination of high-J lines instead. Under these circumstances, the rotational temperature is used to scale all the absorption coefficients to the same J value (generally J=19). This eliminates rotational effects when comparing vibrational band measurements.

3.2.1 Rotational Temperatures

Due to extremely fast rotational relaxation rates in N_2O , on the order of $10^7 \text{ s}^{-1}\text{Torr}^{-1}$ (Section 2.3), the rotational temperature is assumed to be in equilibrium with the background gas temperature. Methods customarily used in gas temperature sensing, including acoustic measurement of the velocity of sound in the gas, direct thermocouple and thermometer detection, and microphonic monitoring of gas pressure changes, are all unsatisfactory for use in gas laser discharges.⁵⁸ A more suitable method examines the distribution of rotational lines of the laser-active molecule itself by measuring the absorption coefficients of several rotational transitions in the same vibrational band.^{16,54,58} The profile of the P and R branches of the rotational-vibrational spectrum is governed solely by the rotational temperature T of the molecule. This is apparent from the ratio of the absorptivities of two different rotational lines of the same vibrational band:

$$\frac{\alpha_{ij}^{\ell_k}(J')}{\alpha_{ij}^{\ell_k}(J)} = K(J,J') \exp -[F(J') - F(J)]/kT. \quad (30)$$

FIGURE 3.3 Rotational distributions measured in the 00^0_0 band of $^{15}\text{N}^{14}\text{N}^{16}\text{O}$ at room temperature, and the 00^0_2 band of $^{14}\text{N}_2^{16}\text{O}$ at a discharge current of 25 mA. The pressure was 13.7 Torr. The smooth curves show the theoretical calculations; the distributions are normalized to a maximum value of unity.



The vibrational factors are identical for numerator and denominator, and the exponential expression depends only on T . The factor $K(J,J')$ includes the effects of the lineshape functions, rotational statistical weights and S_J factors. F is the expression for rotational energy. The foregoing relationship between different J lines of the same band allows normalization of the theoretical spectrum to the experimentally measured points to determine the temperature for which closest agreement occurs. Figure 3.3 presents experimentally measured rotational distributions for two different bands under room temperature and high excitation conditions. The latter curve shows the shift in peak absorption to higher J as the temperature increases. Typically, the fitting procedure determines rotational temperatures to an accuracy of $\pm 10K$. Within this experimental error, different vibrational bands are found to have the same rotational temperature when measured under identical discharge conditions.

3.2.2 Vibrational Temperatures

The vibrational mode temperatures established in a laser discharge are sensitive monitors of the small-signal gain achievable in the system, because they indicate the relative effectiveness of the excitation and de-excitation mechanisms governing population in the vibrational levels. The only previous investigation of the type presented in this thesis was performed on the CO_2 system. Before the advent of the TDL technique, CO_2 lasers were studied by measuring absorption coefficients on the regular $(00^01 - [10^00, 02^00])$ band lines of the CO_2 laser. However, information concerning only the two levels

involved in the transition was obtained, and it was difficult to determine whether Boltzmann distributions were present in the gas. Fortunately, the tunable diode laser technique allows measurements to be made on any transition in the operating frequency range, and the vibrational mode temperatures are determined from the ratios of the populations in three or more levels of a single mode. The population ratios are given by the ratios of absorption coefficients obtained for the same rotational line in different vibrational bands. Since the rotational temperature is known, absorption coefficients measured on different rotational lines can all be scaled to the same line, for example R(19). Consider the following ratio of absorption coefficients in the 00^01 and 00^00 bands:

$$\begin{aligned} \frac{\alpha(00^01)}{\alpha(00^00)} &= \frac{2[N_{002} - N_{001}]}{[N_{001} - N_{000}]} = \frac{2x_3(x_3-1)}{(x_3-1)} \\ &= 2 \exp(-h\nu_3/kT_3) \\ &= 2 N_{001}/N_{000} . \end{aligned} \quad (31)$$

The lineshape factors, matrix elements, statistical weights, etc., for the two transitions cancel for similar J, leaving the ratio dependent purely on T_3 . The factor of two arises from the dependence of the matrix element on the vibrational level as given by the simple harmonic oscillator approximation.⁵⁰ Similarly,

$$\frac{\alpha(00^02)}{\alpha(00^00)} = \frac{3N_{002}}{N_{000}} . \quad (32)$$

The natural logarithms of such vibrational population ratios are plotted

FIGURE 3.4 Vibrational population distributions in the ν_3 mode of N_2O at discharge currents of 5 mA and 25 mA. Data points are experimental measurements made with the TDL, while the solid line is a linear fit, constrained to pass through the point (0,0). The slope of the line gives the mode temperature, T_3 .

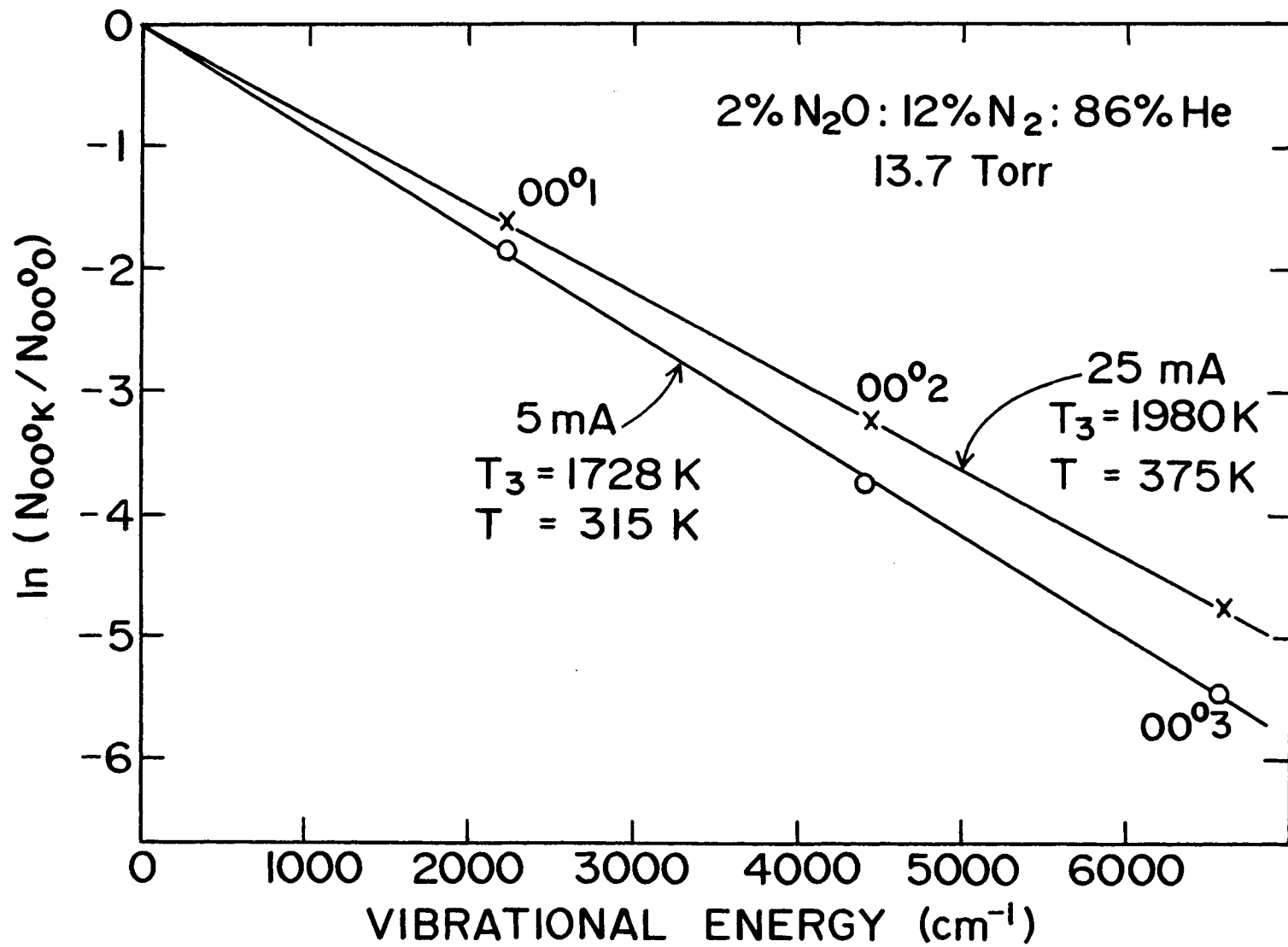
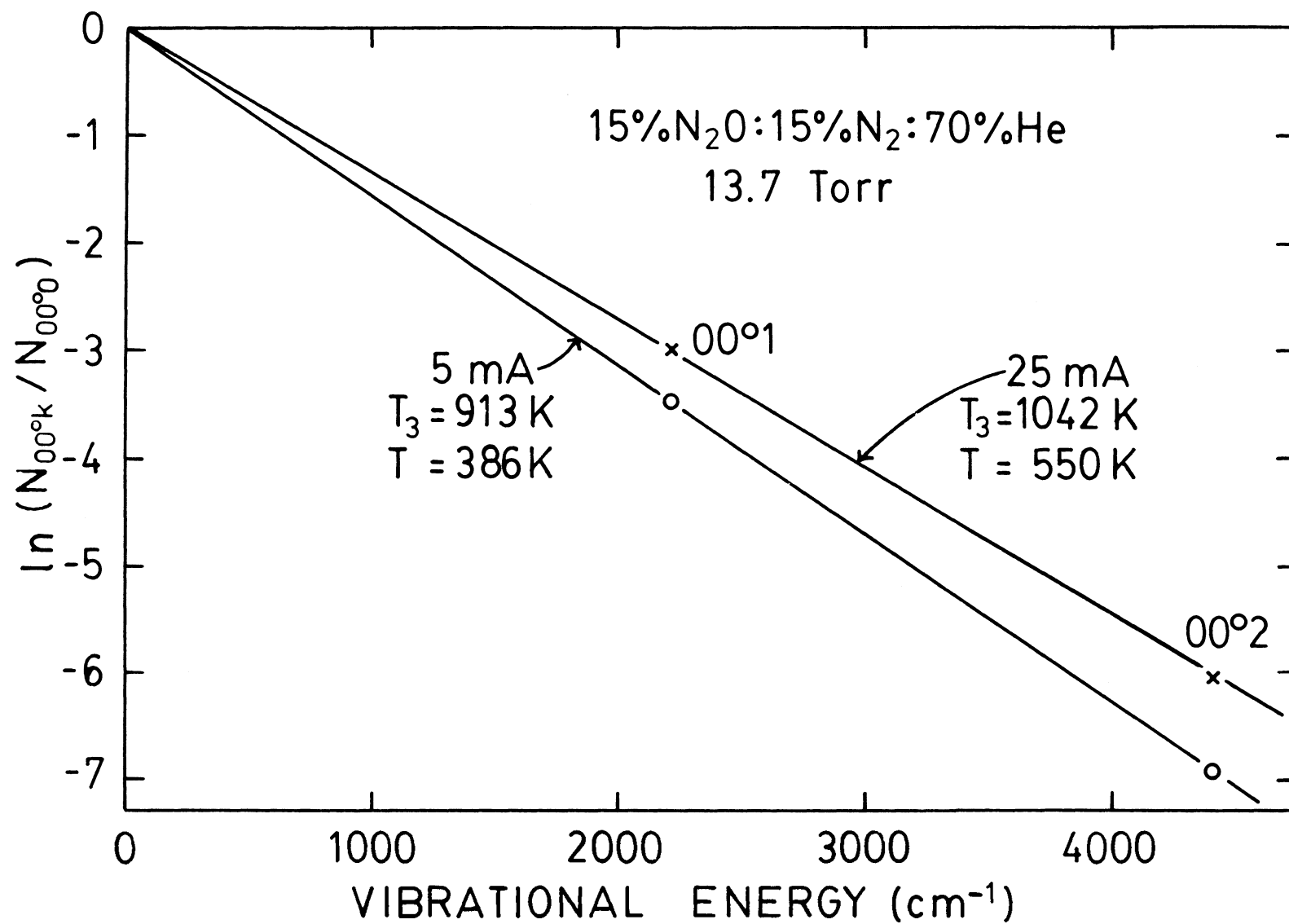


FIGURE 3.5 Repeat of Fig. 3.4 for a 15%N₂O:15%N₂:70%He mixture. Note the drop in T₃ which occurs as the N₂O content is increased from the value of 2% in Fig. 3.4.



versus the known vibrational energy, as in Figs. 3.4 and 3.5. The slope of the resultant line varies as the inverse of the ν_3 mode temperature. To obtain the plots shown in these figures, the value of $\alpha(00^00)$ was adjusted to ensure that the linear least-squares-fit passed through the point (0,0). This procedure was adopted because the measurement of $\alpha(00^00)$ was much more prone to experimental error than the measurement of $\alpha(00^01)$, $\alpha(00^02)$, or $\alpha(00^03)$. (Due to the strength of the fundamental band, the measurement of $\alpha(00^00)$ must be carried out on a high-J line and the measured absorption includes contributions from both discharge and non-discharge portions of the cell.) Note the good fit to a straight line, which indicates that the vibrational population distribution is indeed Boltzmann. In CO_2 it has been found that, for energy levels above those probed in the present experiment, anharmonicity of the CO_2 molecule causes the population distribution to become non-Boltzmann. This effect is not significant for the range of measurements performed here.

The ν_2 mode temperature is calculated as for T_3 , using transitions such as the hotband 01^10 :

$$\begin{aligned} \frac{\alpha(01^10)}{\alpha(00^00)} &= \frac{[N_{011} - N_{010}]}{[N_{001} - N_{000}]} = \frac{x_2(x_3-1)}{(x_3-1)} \\ &= \exp(-h\nu_2/kT_2) \\ &= \frac{N_{010}}{N_{000}} \end{aligned} \quad (33)$$

Assuming simple harmonic behaviour, the general expression for such absorptivity ratios is

$$\frac{\alpha_{ijklk}}{\alpha_{000}} = k x_3^{(k-1)} x_2^j x_1^i . \quad (34)$$

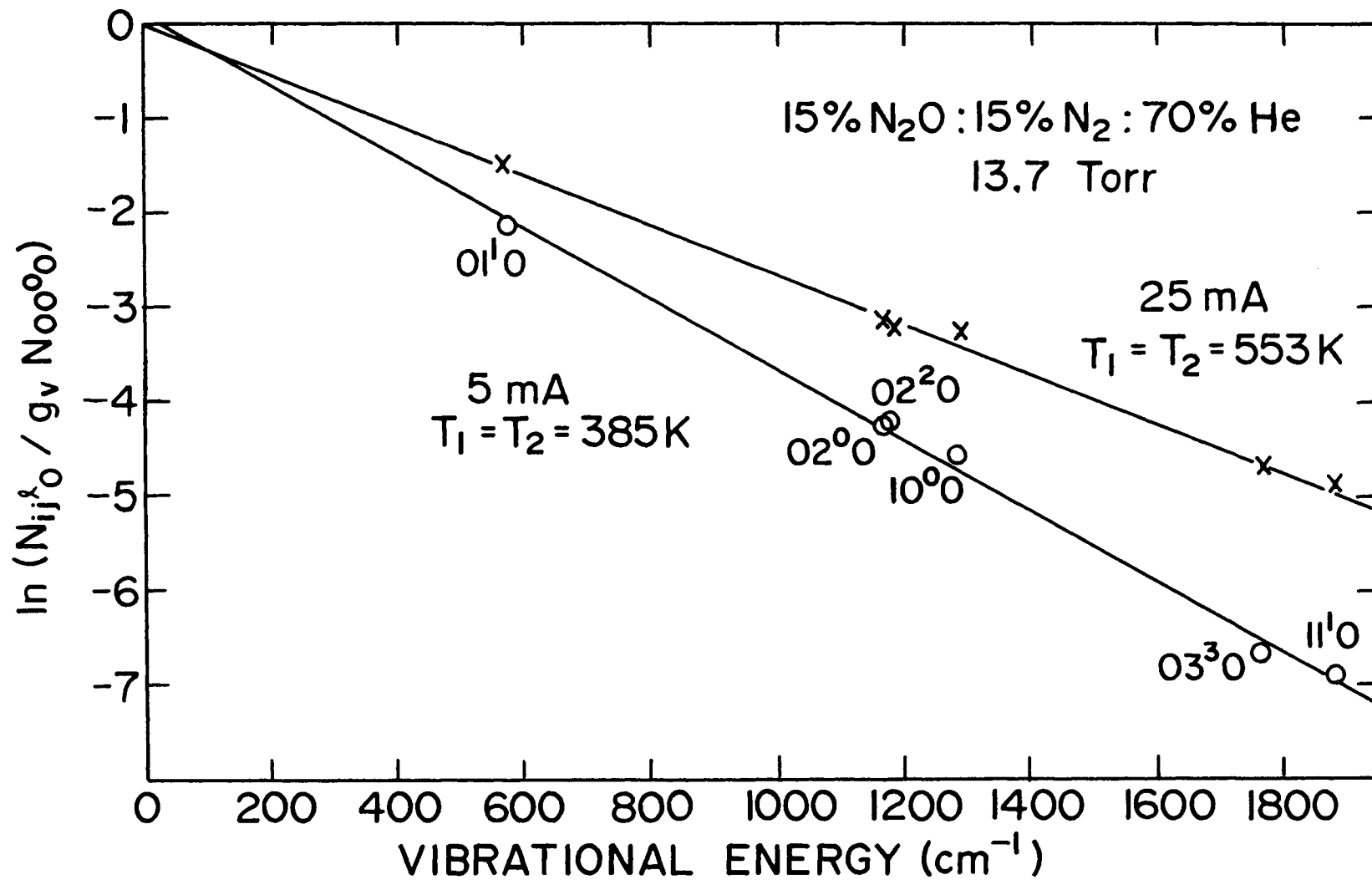
All mode temperatures can thus be determined by choosing the ratios of appropriate vibrational bands.

Typical vibrational distributions for the ν_1 and ν_2 modes are shown in Fig. 3.6. The experimental points included in this figure have been corrected for the absorption which occurs in the non-discharge portion of the discharge tube (see Appendix I). The corrections are significant for the low-lying levels such as 01^1_0 , but have little effect for levels such as 03^3_0 . The fitted value of $\alpha(00^0_0)$, as derived for Figs. 3.4 and 3.5, is used in the calculations of N_{ijklk} . The combined effect of these procedures produces a linear least-squares-fit to the data points which need not pass exactly through the point (0,0) due to scatter in the corrected points. Note that all the ν_1 and ν_2 mode populations lie on the same straight line: i.e., $T_1 = T_2$. A common vibrational mode temperature was observed for all discharge currents, confirming the strong coupling between the modes that has been reported previously.⁴³ In addition, absorption coefficients measured on combination bands such as $(01^1_2-01^1_1)$ are in good agreement with values calculated from the mode-temperature model using T_3 from Fig. 3.5 and T_1 and T_2 from Fig. 3.6.

3.3 Summary

The experimental apparatus and analytic approach involved in measuring mode temperatures and vibrational populations in N_2O has been

FIGURE 3.6 Vibrational population distributions in the ν_1 and ν_2 modes of N_2O at discharge currents of 5 and 25 mA. Data points are experimental measurements for the levels indicated in the figure, while the solid lines represent Boltzmann distributions for the indicated value of $T_1=T_2$.



presented. Calculations of small-signal gain and absorption done using the theoretical mode temperature model are shown to be in agreement with experiment, and the inherent assumptions in the model, including the concept of a Boltzmann distribution for the low-lying vibrational levels, are justified. The ν_1 and ν_2 modes are found to be strongly coupled, with a common vibrational temperature.

CHAPTER 4

DISSOCIATION OF N_2O

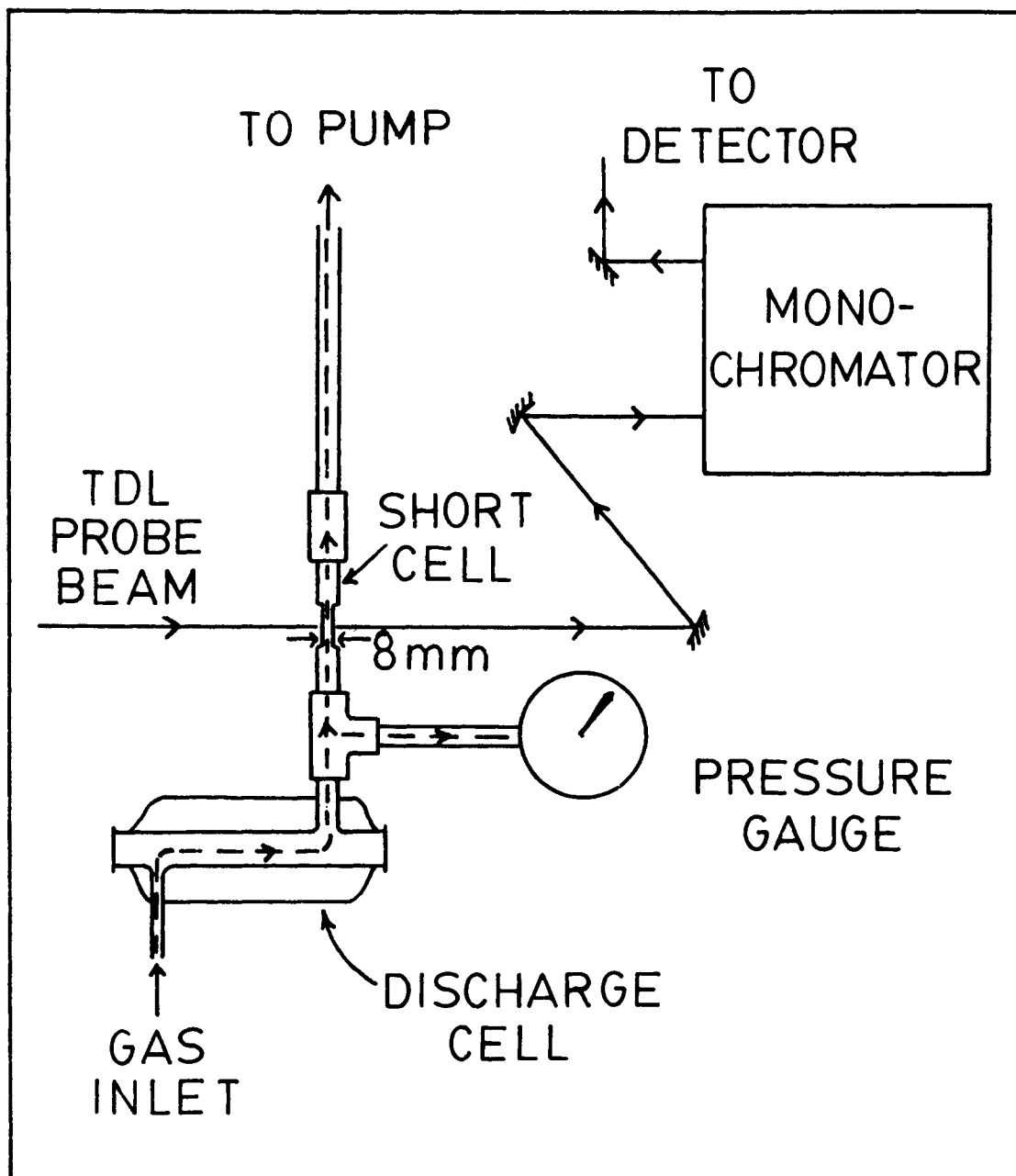
It has long been recognized that dissociation of N_2O plays an important role in the dynamics of N_2O discharges; indeed, it has been proposed as the dominant factor limiting gain in N_2O lasers.^{11,13,14} A measure of the dissociation under a range of mixture and flow conditions is therefore desirable to test this hypothesis, and to ascertain the true gas mixtures corresponding to experimentally determined temperatures.

An approach analagous to the procedure used by Dang et al.¹⁶ to measure dissociation involves monitoring the formation of nitric oxide as N_2O dissociates. Unfortunately, this was not possible as no nitric oxide absorption bands lay within the tuning range of the TDL. Instead, the following technique was used.

4.1 Experimental Procedure

A short gas cell with a window separation of 0.8 cm was inserted into the gas pumping line at the outlet of the discharge tube. The configuration is shown in Fig. 4.1. The TDL was used to monitor absorption on the strong N_2O 00^0_0 lines in this cell. Pressure drop between the gauge and probe point was found to be negligible. As the measured absorption coefficient is proportional to the number of N_2O

FIGURE 4.1 Schematic diagram showing the 0.8-cm-long cell situated at the outlet of the discharge. This short cell is used to measure absorption coefficients on the $^{14}\text{N}^{14}\text{N}^{16}\text{O}$ isotope fundamental lines in order to determine the magnitude of dissociation in the discharge.



molecules present, the degree of dissociation is simply given by the ratio of absorption coefficients measured with and without a discharge current in the primary 14.85-cm cell. For instance, typical results obtained on the P(20) 00⁰0 line show a line centre absorption of 110 %/cm without the discharge, and 64 %/cm with the discharge, revealing that ~40% of the N₂O molecules were dissociated by the discharge. Since Austin and Smith⁵⁹ have indicated that the final dissociation products of N₂O are molecular oxygen and nitrogen, the reformation of N₂O is not expected to be significant. However, the exponential decrease of N₂O along the discharge, as has been shown to occur in CO₂ by Wiegand et al.,⁶⁰ means that dissociation and temperature measurements will only be an average over the range of conditions in the cell. Given that the gas entering the cell is undissociated, and that the fraction f of N₂O molecules remaining as the gas exits the discharge can be determined, the exponential variation in the fraction of N₂O molecules along the length l of the discharge is calculated using

$$f = \exp(-dl) \quad (35)$$

Having found d , the average fraction of the original number of molecules in the discharge is given by

$$f_{av} = 1/dL [1 - \exp(-dL)], \quad (36)$$

where L is the total length of the discharge. This average value f_{av} is used to represent the average gas mixture in the discharge.

Care was taken to verify that the measured change in absorption in the 00⁰0 band was entirely due to dissociation, and not partially

caused by a change in gas temperature or residual v_3 mode excitation. This was accomplished in two ways: (1) it was ascertained that no residual absorption occurred on the strong 00^0_1 excited transition, (2) absorption measurements were made on a number of transitions. For example, the separation of the lower levels of the 00^0_0 P(44) and P(20) transitions is sufficient that agreement in the results obtained with each line confirms that thermal excitation in the gas is not a problem.

4.2 Dissociation Results

The results for net dissociation as a function of current for several flowrates are given in Fig. 4.2. In general, the absolute reproducibility of the dissociation measurements is $\pm 3\%$, regardless of the size of the measured dissociation. As expected, the degree of dissociation increases with increasing current and is found to vary inversely as the gas flow rate. However, in the plot of net dissociation versus mixture in Fig. 4.3, the degree of dissociation also shows a very significant increase at low N_2O concentrations. This behaviour is in agreement with results reported by Austin et al.⁵⁹ It is interesting to note that under the fast flow conditions employed for the data of Fig. 4.3, dissociation is not serious for high concentration mixtures and reasonable currents (<10 mA). These findings contradict the assertion that dissociation is a dominant factor in N_2O lasers. The effects of dissociation on gain are considered in Chapter 6.

The measurements shown in Fig. 4.3 give an estimate of the average N_2O concentration in the discharge, assuming an exponential

FIGURE 4.2 Degree of N_2O dissociation measured at the outlet of the discharge tube as a function of the discharge current and flowrate. The measurements were made on the 00^0_0 P(44) lines of the $^{14}N^{14}N^{16}O$ isotope.

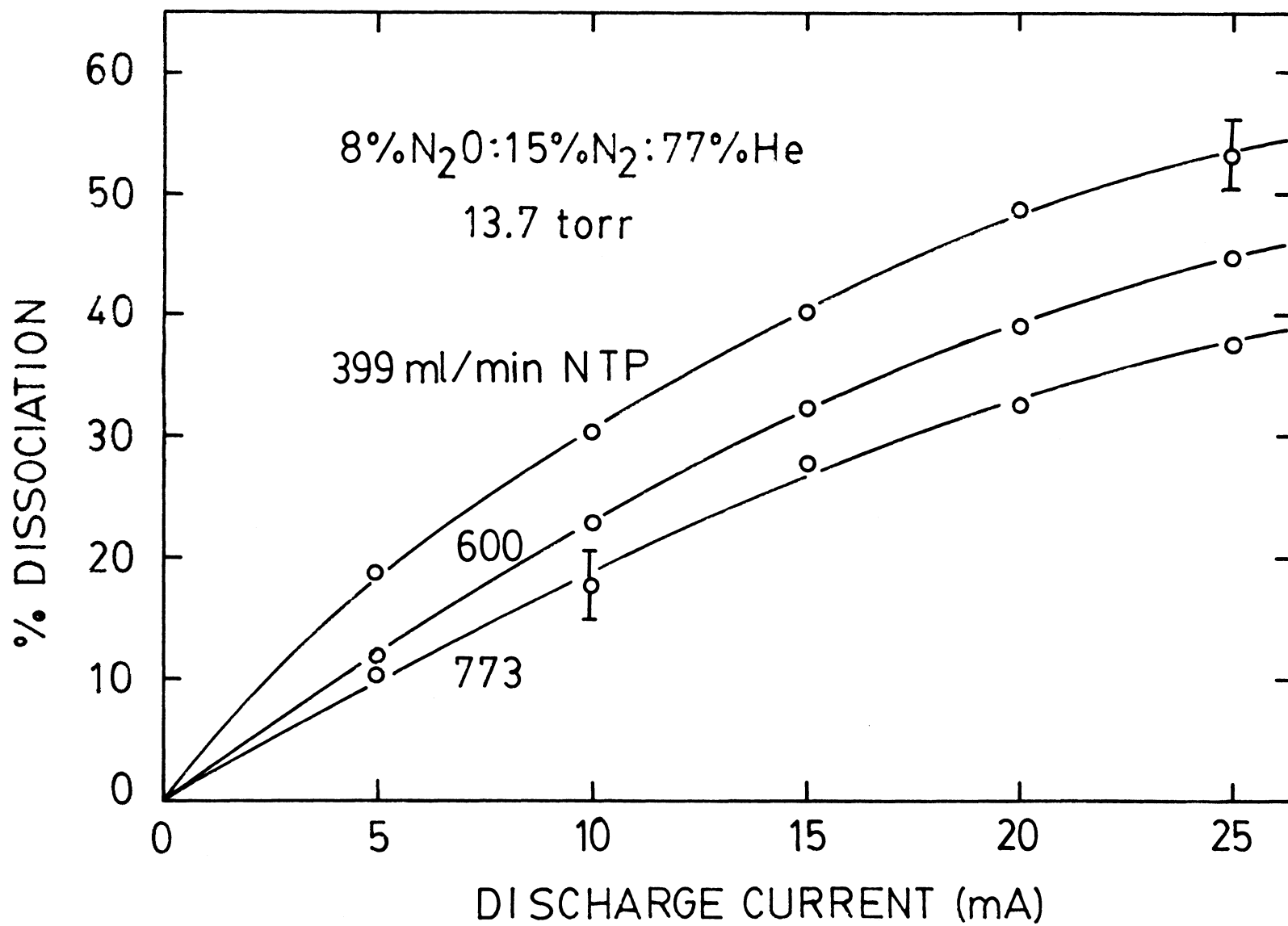
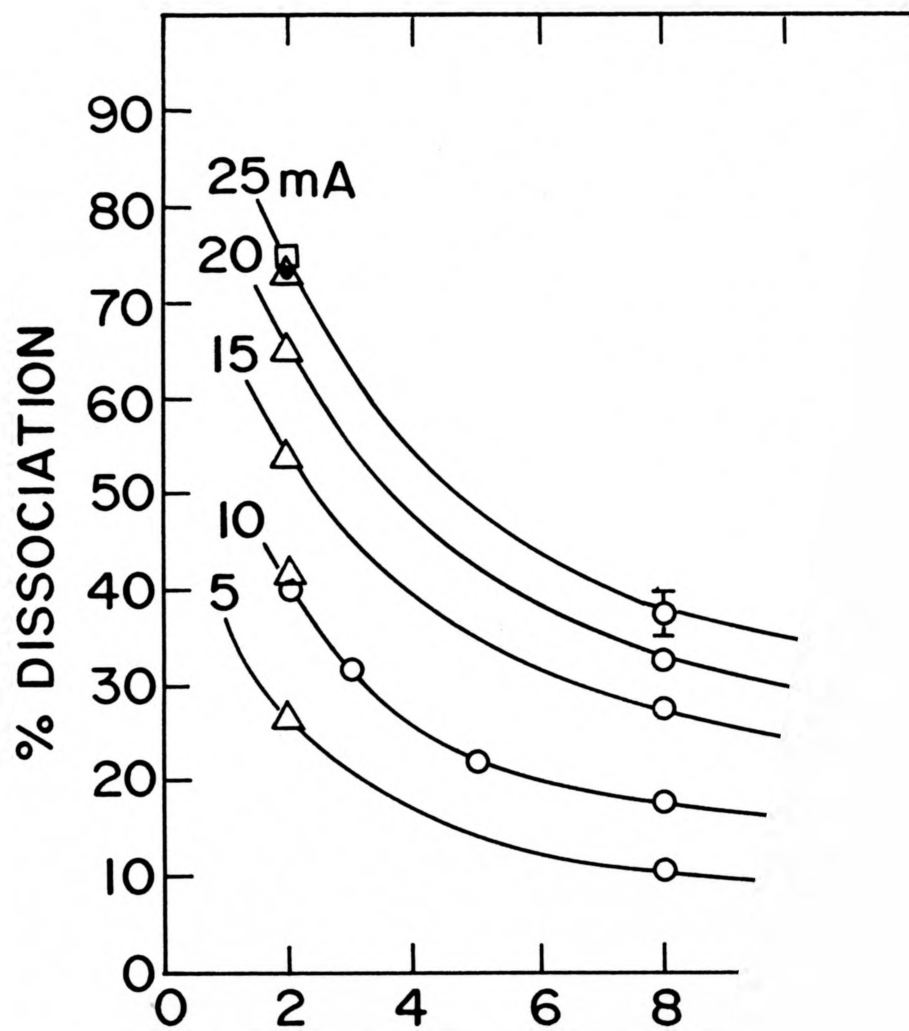
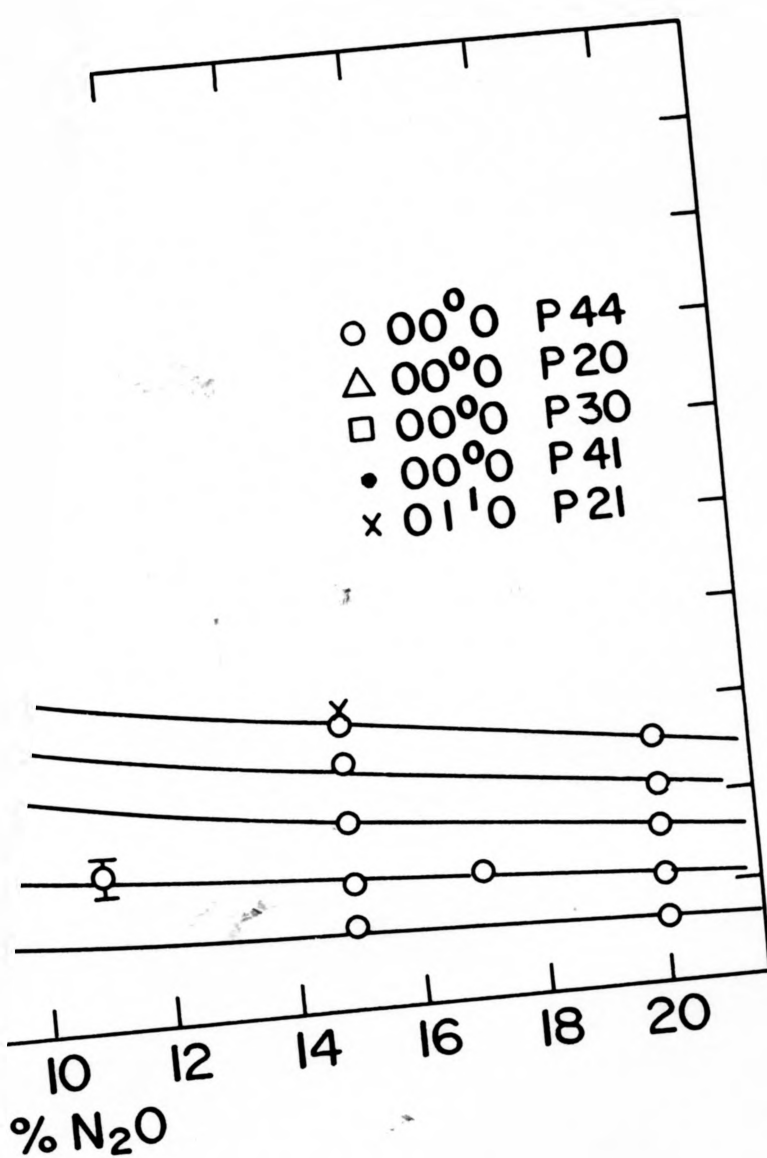


FIGURE 4.3 Degree of N_2O dissociation measured at the outlet of the discharge tube as a function of inlet gas mixture and current. Dwell time in the discharge was ~ 11 msec and the total pressure was 13.7 Torr. The associated absorption measurements were made on a variety of different transitions.





decrease in N_2O along the length of the tube.⁶⁰ Thus, a final check on the self-consistency of the experimental results is possible; the average dissociation can be combined with the measured vibrational and translational temperatures obtained in the next section, and the known gas mixture and pressure, to calculate the absolute absorption coefficients on any N_2O line. Measured absorption coefficients on the excited bands examined in this work are found to agree with the calculated values to within 10%, well within the error introduced by the individual estimates of temperatures and dissociation.

4.3 Summary

A method for measuring net dissociation at the exit of a discharge has been demonstrated. Average dissociation in the discharge can thus be determined, and results agree well with alternative dissociation estimates. From these values, N_2O concentrations under a variety of discharge, current and flow conditions are deduced and used in the following chapter.

CHAPTER 5

MODE TEMPERATURES IN N₂O DISCHARGES

Mode temperatures have been measured for a range of N₂O:N₂:He mixtures, and extensive studies have been made of the 2%N₂O:12%N₂:86%He and 15%N₂O:15%N₂:70%He mixtures. The 15% N₂O mixture was chosen as a typical representative of the gases used in N₂O lasers, while the 2% N₂O mixture exhibits a high T₃. Since the parameter that most strongly influences gain in the N₂O laser is the ν_3 vibrational temperature, its behaviour as a function of current and gas mixture is of special interest.

5.1 Results

The ν_3 vibrational distributions for the two mentioned mixtures were given in Figs. 3.4 and 3.5 of Section 3.2.2 and show that T₃ increases by only 15% between discharge currents of 5 and 25 mA. Figures 5.1 and 5.2 display the variation of the rotational and vibrational temperatures in an N₂O discharge as a function of current for the two mixtures. It is apparent that most of the increase in T₃ occurs at low current and by 15 mA there is clear evidence of T₃ saturation; further increase in current fails to enhance the populations of the ν_3 mode. Saturation is less evident for the ν_1 and ν_2 modes which, to within experimental accuracy, share a common vibrational

FIGURE 5.1 Experimental values of T_3 , $T_2(=T_1)$ and T as a function of discharge current. The gas flow rate is 773 ml/min NTP, resulting in a gas dwell time in the discharge region of ~11 msec.

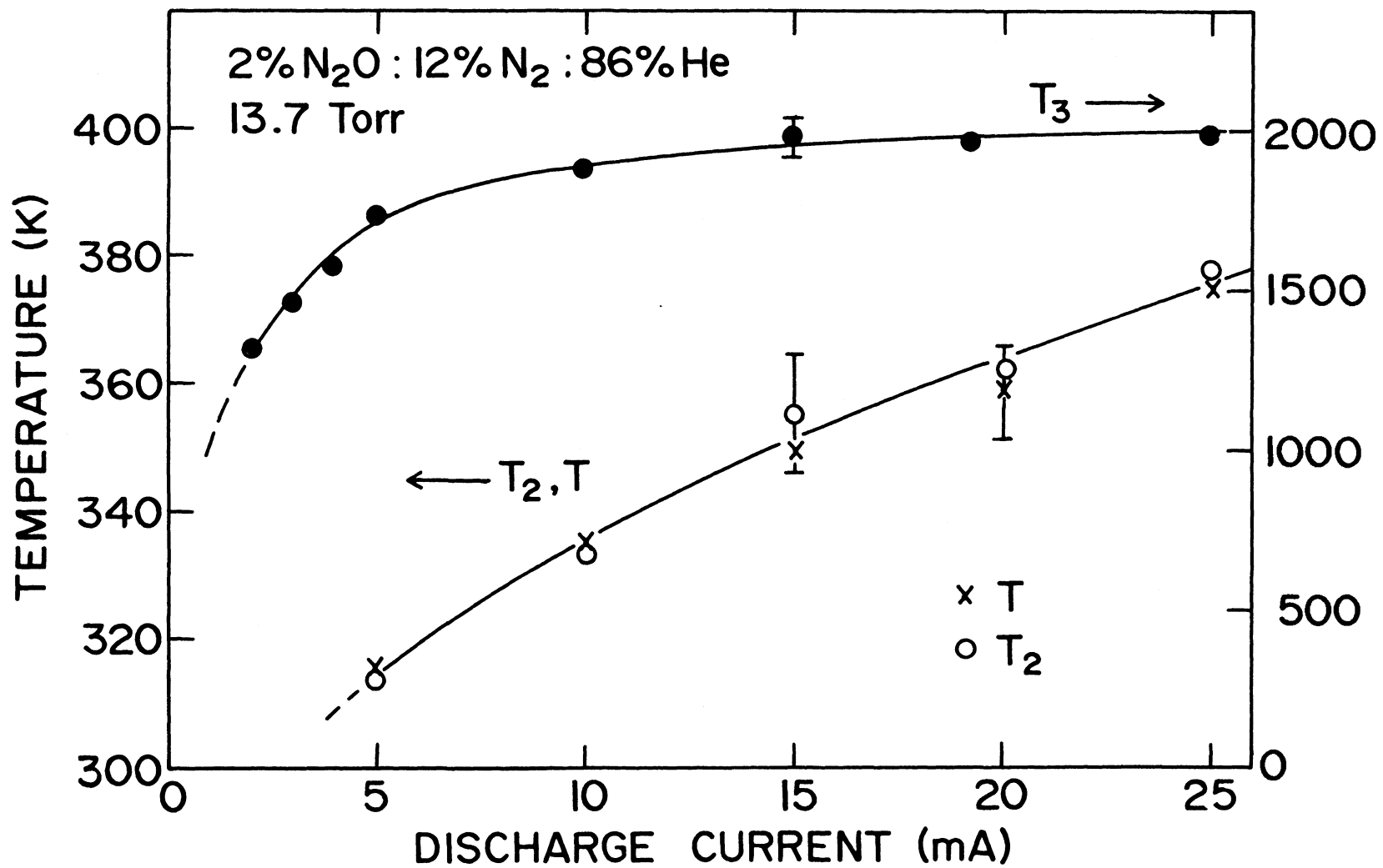
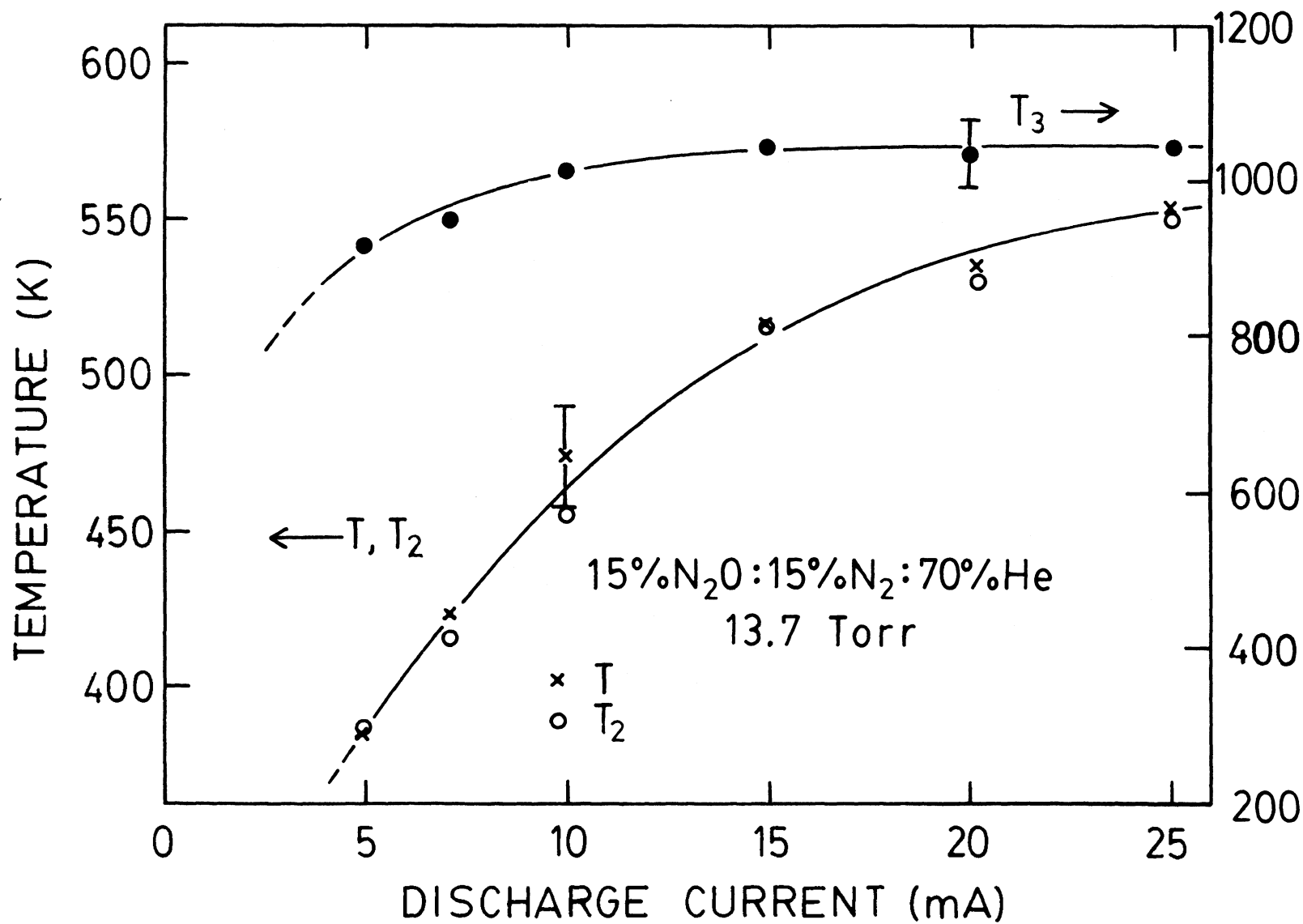
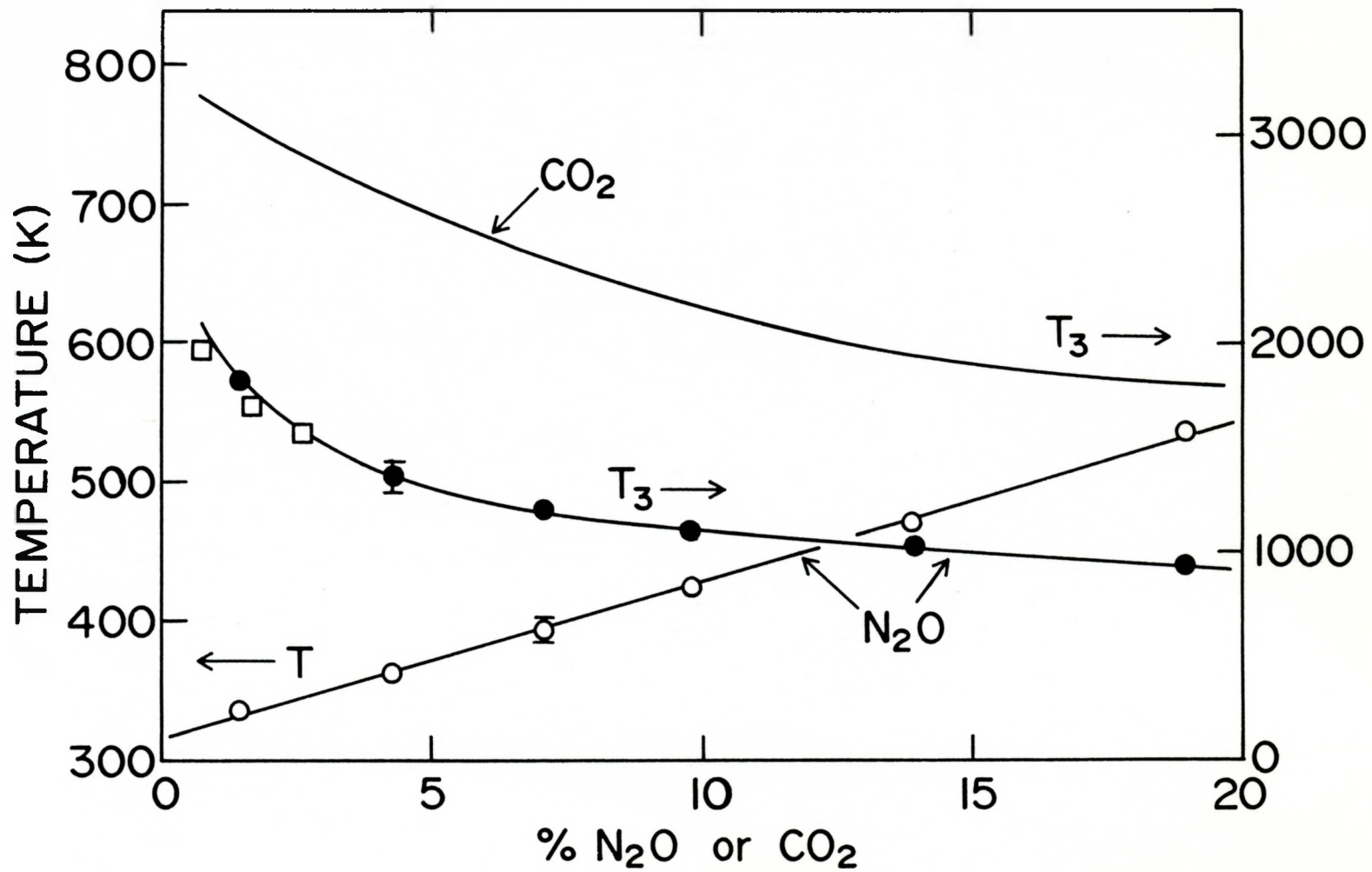


FIGURE 5.2 Repeat of Fig. 5.1 for a 15%N₂O:15%N₂:70%He mixture. The gas flow rate is 399 ml/min NTP, resulting in a gas dwell time in the discharge region of ~21 msec.



temperature. Similar saturation of T_3 has been observed for CO_2 ^{15,16} and has been shown to be caused by electron de-excitation.³⁶ The present measurements indicate that N_2O discharges are even more susceptible to electron de-excitation of the ν_3 mode than are CO_2 discharges. In the 2% N_2O mixture, the maximum T_3 attained is only 2000 K, compared to 3000 K under similar conditions in CO_2 . The limiting value of T_3 in N_2O is smaller, and occurs at a lower current than in the comparable CO_2 case. The relative effects of electron de-excitation in the two gas mixtures can be seen in Fig. 5.3. It should be noted that the dissociation measured at 10 mA (Section 4.2) has been used to correct the mixtures before plotting this figure, e.g. a nominal 2% N_2O mixture dissociates to 1.2% at the outlet of the discharge, and hence the measured T_3 of 1880 K is plotted at an average 1.56% N_2O . Optimum discharge current was taken to be 10 mA, where dissociation is still reasonably low, but T_3 has practically reached its maximum value. As was the case in CO_2 discharges,^{15,16} the maximum attainable value of T_3 in N_2O appears to depend only upon the percent of N_2O , and is independent of the total pressure⁶¹ and the use of pulsed or cw excitation. Thus it appears that electron de-excitation is the primary cause of the poor performance of N_2O lasers. It is noteworthy that a 15% N_2O mixture saturates at a T_3 value of 1000 K with only 3% of the N_2O population in the 00^0_1 level. For the equivalent 15% CO_2 case, T_3 reaches practically 2000 K and ~12% of the molecules are in the 00^0_1 level. It follows that for typical discharge mixtures, the CO_2 laser has almost four times as many molecules in the upper laser level, and consequently the success of the CO_2 laser over the N_2O laser is not

FIGURE 5.3 T_3 measurements as a function of gas mixture in both N_2O and CO_2 discharges. The CO_2 curve is taken from Ref. 63 and represents the average of many pulsed and cw measurements taken under conditions designed to maximize T_3 . The N_2O data points were measured in the present work; the cw measurements (circles) were made with a TDL for a mixture containing 15% N_2 at a total pressure of 13.7 Torr and a discharge current of 10 mA. The pulsed measurements (squares) were made in a transversely-excited discharge using the techniques described in Ref. 63. $T(=T_1=T_2)$ is also shown as a function of gas mixture for N_2O .



surprising.

Gain is also considerably influenced by the background temperature T , which appears in the rotational partition function. To within experimental accuracy, Figs. 5.1 and 5.2 show that $T=T_1(=T_2)$ and the temperature increases steadily with current.⁶² However, T at 25 mA in the 2% N_2O mixture is only 380 K, while in the 15% N_2O gas it has risen considerably to 550 K. This variation in T as a function of gas composition is also indicated in Fig. 5.3. The change in temperature of roughly 200 K across the range of mixtures shown will reduce the N_2O laser gain for rich N_2O mixtures, but a very similar temperature variation is observed in CO_2 discharges.⁶³

5.2 Summary

A systematic examination of mode temperatures has been performed as a function of current in 2% N_2O and 15% N_2O mixtures, and as a function of gas mixture at 10 mA. The rotational/background gas temperature is found to be in equilibrium with the (v_1, v_2) mode temperature, and increases with N_2O concentration. Saturation of T_3 with current is observed to occur at lower temperatures than in CO_2 , and consequently electron de-excitation processes are believed to be more active than in CO_2 discharges. The temperatures obtained in this section are next used to calculate 10- μ m gain.

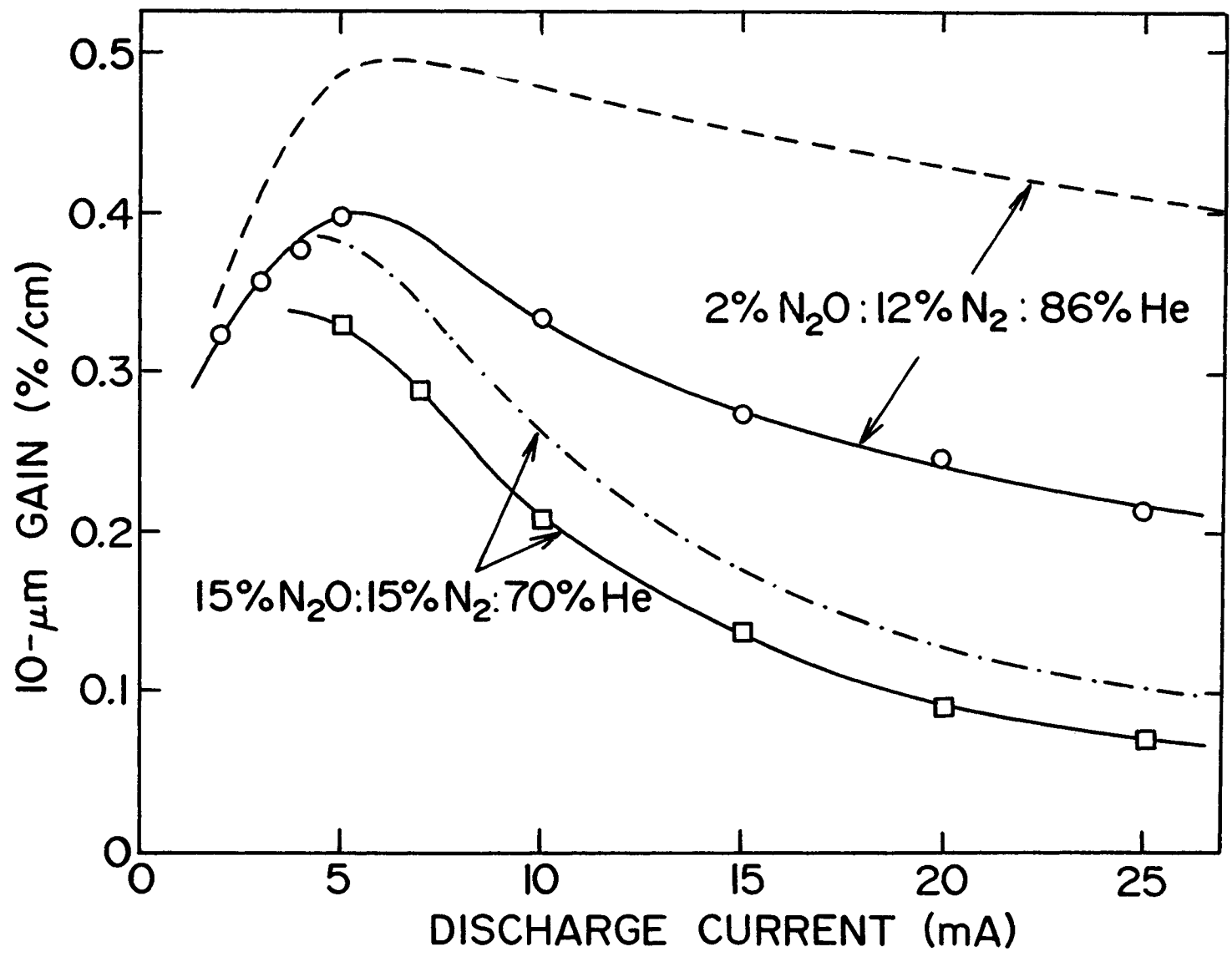
CHAPTER 6

10- μm GAIN CALCULATIONS

6.1 Results

The TDL absorption measurements at 4.5- μm allow the determination of accurate vibrational populations in the 00^01 and 10^00 levels of N_2O . Combining this information with the appropriate vibrational matrix element (0.06 Debye⁴⁹) permits straightforward calculation of the gain on the 10- μm (00^01 - 10^00) laser band. Calculated gain as a function of discharge current is shown in Fig. 6.1 for two different gas mixtures. The temperatures used in these calculations were presented in Figs. 5.1 and 5.2. The calculated points are joined by smooth curves to indicate the 10- μm gain that will be observed under the specified conditions. These results illustrate the relative effects of T_3 , T and dissociation upon the 10- μm gain. At currents above 5 mA, the marginal increase in T_3 cannot compensate for the detrimental effect of increasing T , and thus gain decreases. This reduction in gain is more severe for the 15% N_2O mixture, in which the increase in T between 5 and 25 mA is much greater. In contrast, the effects of dissociation are more serious for the 2% mixture (Fig. 4.3). It should be noted that for the 15% mixture, dissociation plays a minor role in the 10- μm gain dynamics. However, since gain varies directly as N_2O density, but depends exponentially on T_3 , gain for the 2% mixture is greater than in

FIGURE 6.1 Calculated 10- μm gain on the P(20) transition of the $00^0_1-00^0_0$ band for two different N_2O mixtures at 13.7 Torr. The solid lines join calculated points for which dissociation is included; the dashed lines show gain calculated by assuming that the measured temperatures correspond to the undissociated mixtures. Dissociation estimates are an average over the 10-cm discharge length, as outlined in Chapter 4.



the 15% mixture due to significantly higher T_3 .

The variation of gain as a function of gas mixture is shown in Fig. 6.2. Average N_2O concentration in the discharge is estimated from the measured dissociation at the gas outlet, as described in Chapter 4. The average value is then used in the gain calculations and for the abscissa of Fig. 6.2. The net effect of dissociation is to alter the gas composition and hence the associated mode temperatures that influence gain. Thus, provided the actual N_2O content of the mixture is known, this figure gives gain coefficients for both dissociated and undissociated N_2O mixtures.

6.2 Discussion

The measured values of dissociation and mode temperatures can be used with the mode-temperature model to demonstrate the relative effects of these factors on 10- μm gain. Table 6.1 compares the influence of dissociation and T_3 -saturation on 10- μm gain for two gas mixtures in the N_2O and CO_2 systems. It is clear from this table that saturation of T_3 is the dominant mechanism accounting for the difference in N_2O and CO_2 gain coefficients, particularly for the 15% mixtures. The low gain coefficients attainable in N_2O dictate that, in general, the N_2O laser is operating near threshold. Thus, the optical efficiency is low and only the strongest lines in a vibrational band can lase, with the result that the output powers of these lasers are low, and the line tunability limited. Typically, the 10- μm output power produced by a flowing gas laser will drop by a factor of four when N_2O is substituted for CO_2 in

FIGURE 6.2 Calculated 10- μm gain as a function of effective % N_2O in the gas mixture at 13.7 Torr. The mixtures were prepared with 15% N_2 and the balance was helium. The associated TDL measurements were taken at a discharge current of 10 mA, and the calculations were carried out using the data of Figs. 4.3 and 5.3.

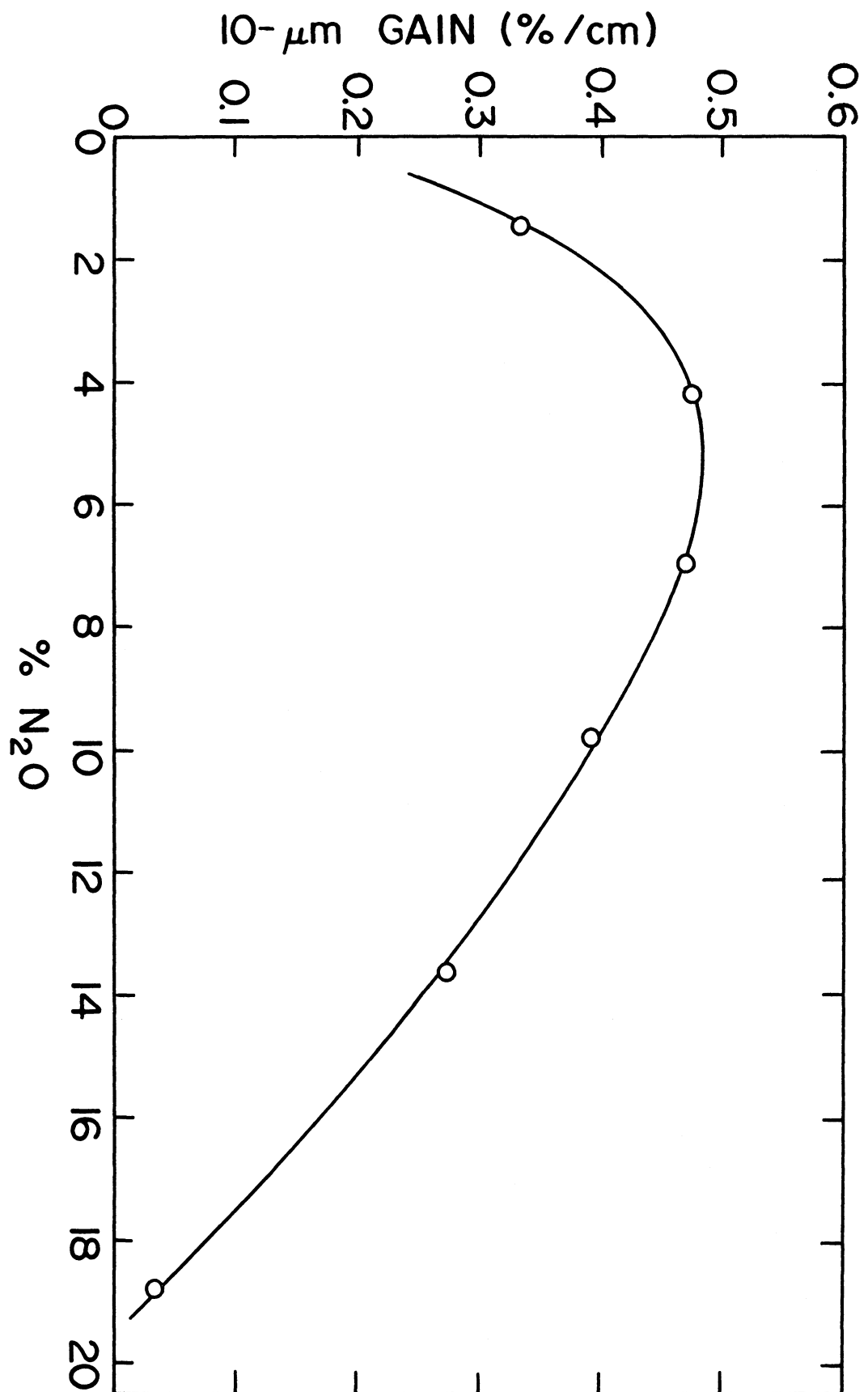


TABLE 6.1
 Comparison of 10- μ m Gain in cw
 N_2O and CO_2 Systems

Conditions	α (%/cm)	α (%/cm)
	F(20)	F(20)
	15% CO_2 :15% N_2 :70%He	15% N_2O :15% N_2 :70%He
$T=T_1=T_2=490K$ ^(a)		
$T_3=1950K$	1.38	1.52
$T=T_1=T_2=490K$	—	
$T_3=1950K$		1.34
$\sim 9\%$ dissociation of N_2O		
$T=T_1=T_2=490K$ ^(b)		
$T_3=1040K$	—	0.22
(incl. dissociation)		
	2% CO_2 :15% N_2 :83%He	2% N_2O :15% N_2 :83%He
$T=T_1=T_2=350K$ ^(a)		
$T_3=3150K$	0.64	0.67
$T=T_1=T_2=350K$	—	
$T_3=3150K$		0.50
$\sim 25\%$ dissociation of N_2O		
$T=T_1=T_2=350K$ ^(b)		
$T_3=1830K$	—	0.31
(incl. dissociation)		

(a) Typical conditions for a CO_2 mixture.

(b) Typical conditions for an N_2O mixture

the gas mixture.⁶⁴

Generally, N_2O lasers have discharge lengths of >100 cm, and consequently the gas molecules tend to remain in the discharge significantly longer than is the case for the work reported here. Dissociation will be more of a problem in these lasers, but the evolution of the gain along the discharge length is still described by the curve in Fig. 6.2. For example, a practical laser may be operated with a nominal gas mixture of 10% N_2O , which dissociates to only 3% at the exit of the discharge. As shown in Figs. 5.3 and 6.2, the reduction in N_2O concentration along the discharge length is offset by an increase in T_3 , and the average gain coefficient will be ~ 0.43 %/cm. Clearly, the optimum gas mixture for a given laser will depend to a large extent upon the gas dwell time and the discharge current. This explains the variety of N_2O laser mixtures quoted in the literature. One successful approach to controlling gas mixture has employed several short sections of tube within the laser feedback elements, each with its own gas inlet and outlet ports.⁶⁵ However, even when an optimum gas mixture is maintained, the gain does not significantly exceed that obtained for the lasers described above.

This work predicts maximum gain for N_2O concentrations of roughly 3 to 8%. Below this region, high T_3 values are balanced by low N_2O number density, while for rich N_2O mixtures, the low T_3 and high T values are responsible for low gain. On the basis of Fig. 6.2, the maximum gain coefficient expected in cw $N_2O:N_2:He$ mixtures is ~ 0.5 %/cm. This result agrees with direct $10\text{-}\mu\text{m}$ small-signal gain measurements made under similar conditions in which a peak gain of ~ 0.43 %/cm was

observed.⁶⁵ The results are also consistent with a peak gain of 0.24 %/cm observed by Djeu et al.¹³ under cw excitation and 0.32 %/cm measured by Mullaney et al.¹² with pulsed excitation. In addition, the variation of 10- μm gain with current shown in Fig. 6.1 is in good agreement with measurements on operating N_2O lasers.⁶⁵

The low values of T_3 in pulsed N_2O discharges are also responsible for the failure of attempts to produce an optically pumped 4.5- μm N_2O laser.⁶⁶ This system relies upon discharge excitation to populate the N_2O 00^0_2 level prior to transferring the population to the 10^0_1 level by means of an optical pulse. The excitation of the ν_3 mode in N_2O is so poor that the population transferred from 00^0_2 to 10^0_1 is insufficient to establish an inversion between the 10^0_1 and 10^0_0 levels. Although lasing is not observed in N_2O , the presence of an inversion in CO_2 mixtures leads to high small-signal coefficients at 4.3 μm .^{67,68} This is a consequence of the strong matrix element for the 10^0_1 - 10^0_0 transition.

The saturation of T_3 is linked to rapid electron de-excitation rates in N_2O which reduce the equilibrium population in the upper laser level.³⁶ Unfortunately, the electron energy distribution in the system is determined primarily by the gas mixture and pressure.⁶⁹ Since the mixture/pressure regime for which lasing occurs is very limited, chances of alleviating the de-excitation problem in a discharge-excited situation are small.

6.3 Summary

Upon the basis of the previously obtained mode temperatures, this section has presented calculations of 10- μm N_2O laser small-signal gain as a function of discharge current and mixture. N_2O laser gain is significantly lower than that of the CO_2 laser, and attains a maximum value of ~ 0.5 %/cm at N_2O concentrations of 3 to 8%. Low T_3 values represent the primary limitation on N_2O laser gain, while dissociation plays only a minor role for conventional laser gas mixtures.

CHAPTER 7

CONCLUSIONS

A summary of the salient features of the present study of cw N_2O laser dynamics is presented in this final chapter, along with a discussion of further investigation and development possible for the N_2O laser. The goal of the work presented in this thesis was to explain the differences in output powers and small-signal gain coefficients observed in N_2O and CO_2 cw lasers. Due to the similarities between the N_2O and CO_2 systems, the TDL technique previously used for a comprehensive study of CO_2 gain dynamics¹⁶ was applied to N_2O . By combining measured absorption coefficients involving more than 18 selected vibrational levels with a theoretical mode-temperature model for populations (Chapter 2), vibrational populations and temperatures can be obtained. This approach to the investigation of the dynamics of N_2O laser discharges has proved to be extremely powerful. Not only has the validity of the mode-temperature model for N_2O been demonstrated, but it has also been shown that the ν_1 and ν_2 modes in N_2O are strongly coupled despite the absence of Fermi resonance between the 10^00 and 02^00 levels. Furthermore, $T_1(=T_2)$ is found to be in equilibrium with the background gas temperature (Chapter 3).

Prior to this study, the gain differences between the CO_2 and N_2O systems were often attributed to dissociation. This contention was investigated in Chapter 4. Significant dissociation of N_2O is shown to

occur in typical cw discharges, particularly at high currents and low concentrations of N_2O . However, under discharge conditions where one might expect to observe maximum 10- μm gain (<10 mA, 10 to 20% N_2O), dissociation plays a minor role.

The most significant result established in this thesis is the saturation of the vibrational temperature T_3 with increasing discharge current (Chapter 5). Such saturation, which is attributed to electron de-excitation,³⁶ severely limits the population that can be established in the 00⁰1 upper laser level. Although the effect is also observed in CO_2 , the attainable T_3 values in N_2O are much lower. The influence of mode temperatures on gain are investigated in Chapter 6. From these calculations, it is evident that T_3 -saturation is the principal factor responsible for the poor performance of N_2O lasers relative to CO_2 lasers.

For all practical purposes, the information presented in this thesis is sufficient for the typical laser user. However, this work has only considered vibrational populations in N_2O discharges under conditions of small-signal 10- μm gain. Similar TDL techniques can be used to examine N_2O saturation dynamics in the presence of strong 10- μm laser fields.^{19,36} By perturbing the population of a level and measuring the rate of return to equilibrium, relaxation mechanisms and electron excitation and de-excitation processes can be also studied.^{36,71} Should it be deemed worthwhile, this information can be used in the modelling of N_2O lasers.

Some workers have chosen to completely avoid discharge excitation in favour of techniques such as optical pumping with resonant

energy transfer between molecules,⁷² or gasdynamic processes where conventional cw N_2O radiation is amplified by a shock-heated N_2O mixture that is adiabatically expanded through a nozzle.⁷³ In addition, multi-atmosphere electron-beam-controlled lasers have been demonstrated.⁷⁴ Although these techniques are not in common use, avenues are obviously still open for the future development of the N_2O laser.

In conclusion, the work described in this thesis has provided a detailed explanation for the low output powers and poor overall performance of the N_2O laser. Although saturation of T_3 appears unavoidable as long as discharge excitation of the laser gas is used, the presented results have indicated the measures required to maximize N_2O laser gain.

APPENDIX I

ANALYSIS OF T_2 DATA

The analysis of absorption data pertaining to the ν_2 vibrational mode is complicated by the non-zero absorption coefficients of many of the lines in the absence of a discharge. Although it is possible to estimate T_2 from several lines involving little or no non-discharge absorption (e.g., from the ratio $01^1_1/00^0_1$ or from the 030 and 110 lines), a vibrational population distribution for a number of energy levels conclusively shows whether or not a single mode temperature exists.

In this work, the absorptivity of a line in the discharge alone is extracted from the experimental measurement of the absorption coefficient as follows. For convenience, the gas cell is divided into two regions: the 10-cm length between the discharge electrodes, and a non-discharge region representing the two ends of the cell that lie outside of the electrodes. An effective length x for the region outside of the discharge and a net dissociation factor D are defined, such that

$$\alpha_{\text{meas}}^{\lambda} = D[\alpha_{\text{nd}}x + \alpha_{\text{d}}(10)] . \quad (\text{I.1})$$

In this formula, α_{nd} refers to the absorption in the non-discharge region, α_{d} is the absorption in the discharge, and $\alpha_{\text{meas}}^{\lambda} = -\ln(I/I_0) \times 100$ is taken directly from the X-Y recorder scans of the line. All absorption coefficients are expressed in %/cm. Once x and D are

determined, they can be substituted into formula (I.1) with the measurements on the line in question to evaluate α_d . Sample calculations are included with the step-by-step procedure outlined below.

To determine D, a fundamental line such as 00^00 (R19) is examined. Normally, the discharge absorptivity $\alpha_{\text{exp}}(\text{R19})$ (including dissociation) of this line is established by the intercept of the vibrational distribution for the corresponding ν_3 data. The rotational temperature and T_3 in the discharge are known from previous measurements and a good estimate of T_2 is given by the ratio $01^11/00^01$. Hence the absorptivity in the discharge without dissociation, $\alpha_{\text{theory}}(\text{R19})$, can be calculated and the difference between the two absorptivities is due to dissociation:

$$\alpha_{\text{theory}}(\text{R19}) \times D = \alpha_{\text{exp}}(\text{R19}) \quad (\text{I.2})$$

This effective dissociation factor is normally in close agreement with other estimates of dissociation for the given mixture and current.

e.g. $15\%N_2O:15\%N_2:70\%He$, 25 mA current, dwell time ~ 21 msec.

From the analysis of the T_3 data, the absorption coefficient for the fundamental R(19) line is

$$\alpha_{\text{exp}}(\text{R19}) = 135 \text{ \%/cm.}$$

From previous measurements,

$$T = 550 \text{ K, } T_1 = T_2 = 550 \text{ K, } T_3 = 1042 \text{ K.}$$

$$\text{Thus } \alpha_{\text{theory}}(\text{R19}) = 198.4 \text{ \%/cm,}$$

and therefore, $D = 0.68$.

A dissociation of 46% is measured at the outlet of the cell. This gives an average dissociation factor of 0.74, as calculated by the method of Chapter 4.1, and is in reasonable agreement with the value derived above.

Next, several measurements on 00^0_0 lines of less abundant isotopes are made, since the main isotope lines are generally too strong to accurately measure. These values are used with D , α_d and α_{nd} to determine an average x factor, where the calculation of α_{nd} requires that an effective temperature for the non-discharge region be estimated. The value chosen is not extremely critical, since the derived x changes somewhat to compensate for a change in temperature - a reasonable estimate is ~ 260 K. The x value also reflects the difference in number density of N_2O molecules in and out of the discharge, as established by dissociation.

e.g. Equation (I.1) can be written for the following five 00^0_0 $^{15}N^{14}N^{16}O$ absorption lines.

<u>Line</u>	<u>Equation</u>	<u>x</u>
P(7)	$11.81 = 0.68[2.91 x + 0.36 (10)]$	4.73
P(8)	$13.01 = 0.68[3.22 x + 0.40 (10)]$	4.69
P(25)	$17.05 = 0.68[2.79 x + 0.69 (10)]$	6.53
P(29)	$12.61 = 0.68[1.98 x + 0.63 (10)]$	6.18
R(23)	$18.96 = 0.68[3.31 x + 0.74 (10)]$	6.17
		$D=0.68, x_{av}=5.66$

At this point, the derived D and x are used with measurements of α_{meas}^l and calculations of α_{nd} on rotational lines of the transition in

question to determine α_d . These results are scaled to the same line using the rotational temperature. An indication of the quality of the measurements and analysis is given by the scatter in these resultant values. Naturally, the required corrections are least for lines with small non-discharge absorption coefficients. After multiplying by the D factor, the result is the desired absorptivity in the discharge. The absorption coefficients are converted to population differences and the natural log of the ratios $\alpha_{ij}^k/\alpha_{000}$ are plotted as in Fig. 3.6, forming a vibrational distribution.

e.g. 10^0-10^1 band

<u>Line</u>	<u>Equation</u>	<u>α_d</u>
P(8)	$30.04 = 0.68[0.72(5.66) + 10\alpha_d]$	4.01
P(14)	$44.07 = 0.68[0.92(5.66) + 10\alpha_d]$	5.96
P(27)	$46.10 = 0.68[0.51(5.66) + 10\alpha_d]$	6.49

Note that the corrections to the absorption coefficients, as given by the first term in square brackets, are less than 10% of the derived 'true' absorption coefficients represented by the second term in square brackets.

After multiplying by the dissociation factor, the lines are scaled to R(19). The values for the absorption coefficient in the discharge are:

$$\begin{aligned}\alpha_d(R19) &= 4.94 \text{ (as derived from P(8)).} \\ &= 4.86 \text{ (" " " P(14)).} \\ &= 4.96 \text{ (" " " P(27)).}\end{aligned}$$

$$\alpha_{av}(R19) = 4.92$$

$$\text{Therefore, } \ln(\alpha_{100}/\alpha_{000}) = -3.31$$

The results of this sample calculation are plotted in Fig. 3.6 at a vibrational energy of 1284.9 cm^{-1} .

All data analysed using this procedure is consistent with other calculations of T_2 , and shows that a Boltzmann distribution is present in the N_2O gas mixture.

REFERENCES

1. B.G. Whitford, K.J. Siemsen, H.D. Riccius, "Saturated-absorption-stabilized N₂O laser for new frequency standards," *Atomic Masses Fund. Const.* 5, 378-382 (1976).
2. F. Shimizu, "Stark Spectroscopy of ¹⁵NH₃ ν₂ Band by 10-μ Lasers," *J. Chem. Phys.* 53, 1149-1151 (1970).
3. T.E. Gough, D.G. Knight, G. Scoles, "Matrix spectroscopy in the gas phase: IR spectroscopy of argon clusters containing SF₆ or CH₃F," *Chem. Phys. Lett.* 97, 155-160 (1983).
4. T. Oka, T. Shimizu, "Observation of Infrared-Microwave Two-Photon Transitions in NH₃," *Appl. Phys. Lett.* 19, 88-90 (1971).
5. L.E.S. Mathias, A. Crocker, M.S. Wills, "Laser oscillations from nitrous oxide at wavelengths around 10.9 μ," *Phys. Lett.* 13, 303-304 (1964).
6. C.K.N. Patel, "CW laser action in N₂O (N₂-N₂O system)," *Appl. Phys. Lett.* 6, 12-13 (1965).
7. G. Moeller, J. Dane Rigden, "Observation of laser action in the R-branch of CO₂ and N₂O vibrational spectra," *Appl. Phys. Lett.* 8, 69-70 (1966).
8. N. Djeu, G.J. Wolga, "Observation of New Laser Transitions in N₂O," *IEEE J. Quantum. Electron.* QE-5, 50 (1969).
9. B.G. Whitford, K.J. Siemsen, H.D. Riccius, G.R. Hanes, "Absolute frequency measurements of N₂O laser transitions," *Opt. Commun.* 14, 70-74 (1975).
10. D.R. Sokoloff, A. Javan, "Precision Spectroscopy of the N₂O, 00⁰₁-10⁰₀ Laser Band by Frequency Mixing in an Infrared, Metal-Metal Oxide-Metal Point Contact Diode," *J. Chem Phys.* 56, 4028-4031 (1972).
11. K. Siemsen, J. Reid, "New N₂O laser band in the 10 μm wavelength region," *Opt. Commun.* 20, 284-288 (1977).
12. G.J. Mullaney, H.G. Ahlstrom, W.H. Christiansen, "Pulsed N₂O Molecular Laser Studies," *IEEE J. Quantum Electron.* QE-7, 551-555 (1971).

13. N. Djeu, T. Kan, G. Wolga, "Laser Parameters for the 10.8- μ N₂O Molecular Laser," *IEEE J. Quantum Electron.* QE-4, 783-785 (1968).
14. Colin Willett, Introduction to Gas Lasers: Population Inversion Mechanisms (Pergamon Press, Oxford, 1974), p. 301.
15. K.J. Siemsen, J. Reid, C. Dang, "New Techniques for Determining Vibrational Temperatures, Dissociation, and Gain Limitations in CW CO₂ Lasers," *IEEE J. Quantum Electron.* QE-16, 668-676 (1980).
16. C. Dang, J. Reid, B. K. Garside, "Detailed Vibrational Population Distributions in a CO₂ Laser Discharge as Measured with a Tunable Diode Laser," *Appl. Phys. B* 27, 145-151 (1982).
17. B.F. Gordietz, N.N. Sobolev, V.V. Sokovikov, L.A. Shelepin, "Population Inversion of the Vibrational Levels in CO₂ Lasers," *IEEE J. Quantum Electron.* QE-4, 796-802 (1968).
18. C.B. Moore, R.E. Wood, B.-L. Hu, J.T. Yardley, "Vibrational Energy Transfer in CO₂ Lasers," *J. Chem. Phys.* 46, 4222-4231 (1967).
19. C. Dang, J. Reid, B.K. Garside, "Gain Limitations in TE CO₂ Laser Amplifiers," *IEEE J. Quantum Electron.* QE-16, 1097-1103 (1980).
20. G. Herzberg, Molecular Spectra and Molecular Structure II. Infrared and Raman Spectra of Polyatomic Molecules (Van Nostrand, New York, 1947).
21. J.M. Brown, J.T. Hougen, K.-P. Huber, J.W.C. Johns, I. Kopp, H. Lefebvre-Brion, A.J. Merer, D.A. Ramsay, J. Rostas, R.N. Zare, "The Labeling of Parity Doublet Levels in Linear Molecules," *J. Mol. Spectrosc.* 55, 500-503 (1975).
22. J. Pliva, "Molecular Constants of Nitrous Oxide, ¹⁴N₂¹⁶O," *J. Mol. Spectrosc.* 27, 461-488 (1968).
23. C. Amiot, "Vibration-Rotation Bands of ¹⁴N¹⁵N¹⁶O-¹⁵N¹⁴N¹⁶O: 1.6-5.7 μ m Region," *J. Mol. Spectrosc.* 59, 191-208 (1976).
24. C. Amiot, G. Guelachvili, "Extension of the 10⁶ Samples Fourier Spectrometry to the Indium Antimonide Region: Vibration-Rotation Bands of ¹⁴N₂¹⁶O: 3.3-5.5 μ m Region," *J. Mol. Spectrosc.* 59, 171-190 (1976).
25. R. Farrenq, J. Dupre-Maquaire, "Vibrational Luminescence of N₂O Excited by dc Discharge - Rotation-Vibration Constants," *J. Mol. Spectrosc.* 49, 268-279 (1974).
26. R.A. McClatchey, W.S. Benedict, S.A. Clough, D.E. Burch, R.F. Calfee, K. Fox, L.S. Rothman, J.S. Garing, "AFCRL Atmospheric Absorption Line Parameters Compilation," Air Force Cambridge

- Research Laboratory, Mass. (1973).
27. W.L. Nighan, J.H. Bennett, "Electron energy distribution functions and vibrational excitation rates in CO₂ laser mixtures," Appl. Phys. Lett. 14, 240-243 (1969).
 28. W.L. Nighan, "Effect of molecular dissociation and vibrational excitation on electron energy transfer in CO₂ laser plasmas," Appl. Phys. Lett. 15, 355-357 (1969).
 29. G.J. Schulz, "Vibrational Excitation of N₂, CO and H₂ by Electron Impact," Phys. Rev. 135, A988-A994 (1964).
 30. At 400 K, $kT \sim 280 \text{ cm}^{-1}$.
 31. C. Alamichel, A. Picard-Bersellini, "Rate constant of vibrational transfer from the ν_3 mode to the ν_1 and ν_2 modes of N₂O," Chem. Phys. 35, 381-386 (1978).
 32. A. Picard-Bersellini, C. Rossetti, C. Boulet, "A study of vibrational relaxation of nitrous oxide by high resolution infrared emission spectroscopy," Spectrochim. Acta 34A, 1067-1076 (1978).
 33. J.T. Yardley, "Vibration-to-Vibration Energy Transfer in Gas Mixtures Containing Nitrous Oxide," J. Chem. Phys. 49, 2816-2821 (1968).
 34. J. Reid, K. Siemsen, "Laser power and gain measurements on the sequence bands of CO₂," J. Appl. Phys. 48, 2712-2717 (1977).
 35. D.F. Starr, J.K. Hancock, "Vibrational deactivation of N₂O(001) by N₂O, CO, and Ar from 144-405^oK," J. Chem. Phys. 62, 3747-3753 (1975).
 36. C. Dang, J. Reid, B.K. Garside, "Dynamics of the CO₂ Upper Laser Level as Measured with a Tunable Diode Laser," IEEE J. Quantum Electron. QE-19, 755-764 (1983).
 37. W.H. Anderson, D.F. Hornig, "The structure of shock fronts in gases," Mol. Physics 2, 49-63 (1959).
 38. R. Holmes, G.R. Jones, R. Lawrence, "Rotational Relaxation in Carbon Dioxide and Nitrous Oxide," J. Chem. Phys. 41, 2955-2956 (1964).
 39. R.R. Jacobs, K.J. Pettipiece, S.J. Thomas, "Rotational relaxation constants for CO₂," Appl. Phys. Lett. 24, 375-377 (1974).
 40. R. Farrenq, D. Gaultier, C. Rossetti, "Vibrational Luminescence of N₂O Excited by dc Discharge," J. Mol. Spectrosc. 49, 280-288 (1974).

41. J. Finzi, C.B. Moore, "Relaxation of $\text{CO}_2(10^01)$, $\text{CO}_2(02^01)$, and $\text{N}_2\text{O}(10^01)$ vibrational levels by near-resonant V-V energy transfer," *J. Chem. Phys.* 63, 2285-2288 (1975).
42. R.T. Pack, "Analytic estimation of almost resonant molecular energy transfer due to multipolar potentials. VV processes involving CO_2 ," *J. Chem. Phys.* 72, 6140-6152 (1980).
43. A. Picard-Bersellini, C. Rossetti, "Evolution des populations de N_2O excite par l'azote active par spectroscopie d'emission," *Spectrochim. Acta* 32A, 1725-1729 (1976).
44. H. Gueguen, A. Carion, M. Margottin-Maclou, L. Doyennette, "Thermalisation vibrationnelle du protoxyde d'azote et du gaz carbonique excites sur le niveau vibrationnel (00^01) en fonction de la temperature," *C. R. Acad. Sc. Paris* 274, 482-484 (1972).
45. P.K. Cheo, " CO_2 Lasers" in Lasers, Vol. 3, A.K. Levine, A.J. Demaria, eds. (Marcel Dekker, Inc., New York, 1971), p. 170.
46. J. Mellis, A.L.S. Smith, "Gain Limitations in CO_2 Lasers," *Opt. Commun.* 41, 121-125 (1982).
47. A.M. Robinson, "Gain Distribution in a CO_2 TEA Laser," *Can. J. Phys.* 50, 2471-2474 (1972).
48. R.H. Kagann, "Infrared Absorption Intensities for N_2O ," *J. Mol. Spectrosc.* 95, 297-305 (1982).
49. N. Lacombe, C. Boulet, E. Arie, "Spectroscopie par Source Laser. III Intensites et Largeurs des Raies de la Transition 00^01-10^00 du Protoxyde d'Azote. Ecartis a la Forme de Lorentz," *Can. J. Phys* 51, 302-310 (1973).
50. e.g., the square of the vibrational matrix element for the 00^03-00^02 band is assumed to be three times the corresponding value for the 00^01-00^00 band.
51. S.S. Penner, Quantitative Molecular Spectroscopy and Gas Emissivities (Pergamon Press, London, 1959), p. 152.
52. R.K. Brimacombe, J. Reid, "Measurements of Anomalous Gain Coefficients in Transversely Excited CO_2 Lasers," *IEEE J. Quantum Electron.* QE-19, 1674-1679 (1983).
53. B.H. Armstrong, "Spectrum line profiles: the voigt function," *J. Quant. Spectrosc. Radiat. Transfer* 7, 61-88 (1967).
54. R.K. Brimacombe and J. Reid, "Accurate Measurements of Pressure-Broadened Linewidths in a Transversely Excited CO_2

- Discharge," IEEE J. Quantum Electron. QE-19, 1668-1673 (1983).
55. N. Lacombe, A. Levy, G. Guelachvili, "Fourier transform measurement of self-, N₂- and O₂-broadening of N₂O lines: temperature dependence of linewidths," Appl. Opt. 23, 425-435 (1984).
 56. J. Reid, D. Labrie, "Second-Harmonic Detection with Tunable Diode Lasers - Comparison of Experiment and Theory," Appl. Phys. B 26, 203-210 (1981).
 57. For convenience, vibrational bands will generally be identified by the lower level only, e.g., the (00⁰3-00⁰2) absorption band becomes the 00⁰2 band.
 58. L.A. Weaver, L.H. Taylor, L.J. Denes, "Rotational temperature determinations in molecular gas lasers," J. Appl. Phys. 46, 3951-3958 (1975).
 59. J.M. Austin, A.L.S. Smith, "Decomposition of N₂O in a glow discharge," J. Phys. D: Appl. Phys. 6, 2236-2241 (1973).
 60. W.J. Wiegand, M.C. Fowler, J.A. Benda, "Carbon Monoxide formation in CO₂ Lasers," Appl. Phys. Lett. 16, 237-239 (1970).
 61. Little change in T₃ was observed over a pressure range from seven to 14 Torr in the cw discharge, although a slight increase in T toward higher pressure has been observed. The pulsed measurements shown in Fig. 5.3 for N₂O were taken at a pressure of 80 Torr.
 62. Measurements made in CO₂ discharges generally determine T₂ to be ~20 K higher than T,¹⁶ but part of this difference may arise from an under-estimation of T through the use of inaccurate CO₂-He pressure-broadening coefficients.⁵⁴
 63. R.K. Brimacombe, J. Reid, T.A. Znotins, "Gain Dynamics of the 4.3- μ m CO₂ Laser," unpublished.
 64. C. Gastaud, M. Redon, P. Belland, M. Fourier, "Far-infrared laser action in vinyl chloride, vinyl bromide, and vinyl fluoride optically pumped by a cw N₂O laser," Int. J. Infrared Millimeter Waves 5, 875-885 (1984).
 65. Personal communication, Klaus Siemsen, NRC, Ottawa, Canada.
 66. R. K. Brimacombe, Ph.D. Thesis, McMaster University, Department of Physics, Hamilton, Ontario, Canada.
 67. T.A. Znotins, J. Reid, B.K. Garside, E.A. Ballik, "4.3- μ m TE CO₂ laser," Opt. Lett. 4, 253-255 (1979).
 68. T.A. Znotins, J. Reid, B.K. Garside, E.A. Ballik, "4.3- μ m cascade

- CO₂ laser," Appl. Phys. Lett. 39, 199-201 (1981).
69. J.J. Lowke, A.V. Phelps, B.W. Irwin, "Predicted electron transport coefficients and operating characteristics of CO₂-N₂-He laser mixtures," J. Appl. Phys. 44, 4664-4671 (1973).
 70. Personal communication, John Reid, McMaster University, Canada.
 71. C. Dang, J.Reid, B.K. Garside, "Dynamics of the CO₂ Lower Laser Levels as Measured with a Tunable Diode Laser," Appl. Phys. B 31, 163- 172 (1983).
 72. T.Y. Chang, O.R. Wood, "Optical transfer 42-atm N₂O laser," Appl. Phys. Lett. 24, 182-183 (1974).
 73. Y.I. Grin', V.M. Polyakov, V.G. Testov, "Experimental study of gasdynamic amplification of N₂O-N₂-He laser emission," ZhETF Pis. Red. 18, 260-263 (1973).
 74. F. O'Neill, W.T. Whitney, "Continuously tunable multiatmosphere N₂O and CS₂ lasers," Appl. Phys. Lett. 28, 539-541 (1976).